

TRAJECTORY OPTIMIZATION AND GUIDANCE FOR AN AEROSPACE PLANE

Final Report
September 1988 through August 1989

September 1989

LANGLEY
GRANT
IN-05-CR
231728
428

Research Supported by NASA Langley Research Center

NASA Grant Number NAGI-907

Principal Investigator: Kenneth D. Mease
Graduate Research Assistant: Mark A. Van Buren

Department of Mechanical and Aerospace Engineering
School of Engineering and Applied Science
Princeton University, Princeton, New Jersey 08544

NASA Grant Monitor: D. D. Moerder

(NASA-CR-185884) TRAJECTORY OPTIMIZATION
AND GUIDANCE FOR AN AEROSPACE PLANE Final
Report, Sept. 1988 - Aug. 1989 (Princeton
Univ.) 42 p C5CL 01C

N90-13369

Unclas
G3/05 0231728

TABLE OF CONTENTS

ACKNOWLEDGEMENTS.....2

NOTATION.....3

SUMMARY OF WORK COMPLETED.....4

1. INTRODUCTION.....5

2. PROBLEM FORMULATION.....6

 2.1 Equations of Motion.....6

 2.2 Initial and Final Conditions.....7

 2.3 Performance Index.....8

 2.4 State and Control Constraints.....8

 2.5 Optimality Conditions.....8

3. VEHICLE MODELING.....12

 3.1 The Aerodynamic Characteristics.....12

 3.2 The Propulsion System.....12

 3.1.1 The Ramjet.....13

 3.1.2 The Scramjet.....13

 3.2.3 The Rocket.....14

4. SOLUTION APPROACH.....15

5. RESULTS.....16

 5.1 Effect of Acceleration Constraints.....16

 5.2 Effect of Available Thrust Level.....17

 5.3 Effect of Fuel Specific Impulse.....17

6. CONCLUSIONS AND WORK IN PROGRESS.....18

REFERENCES.....19

TABLES.....21

FIGURES.....23

APPENDIX.....33

 A.0 INTRODUCTION.....33

 A.1 AMBIENT AND FREE-STREAM CONDITIONS.....33

 A.2 THE AFTERBURNING TURBOJET.....33

 A.2.1 The Intake.....34

 A.2.2 The Compressor.....34

 A.2.3 The Combustion Chamber.....35

 A.2.4 The Turbine.....35

 A.2.5 The Afterburner.....36

 A.2.6 The Nozzle.....36

 A.3 THE RAMJET.....37

 A.4 THE SCRAMJET.....38

 A.4.1 The Intake.....38

 A.4.2 The Combustion Chamber.....38

 A.4.3 The Nozzle.....39

 A.5 CONCLUSION.....40

ACKNOWLEDGEMENTS

The authors thank the United States Air Force for allowing us to use the OTIS computer program.

NOTATION

A	Cross Section Area
a	Acceleration
C	State and Control Inequality Constraint
C_D	Drag Coefficient
C_L	Lift Coefficient
C_V	Velocity Coefficient
c_p	Constant Pressure Specific Heat
D	Drag Force
ER	Expansion Ratio
f	Fuel to Air Ratio
G	Acceleration Load Limit
g	Gravitational Acceleration
H	Heating Value, Hamiltonian
h	Altitude
I_{sp}	Fuel Specific Impulse
K_D	Process Efficiency
L	Lift Force
M	Mach Number
m	Mass, Mass Flow
p	Pressure
p_x	Adjoint Variable to the State X
Q	Heating Rate
q	Dynamic Pressure
R	Earth Equatorial Radius, Gas Constant Air
r	Radial Distance to the Center of the Earth, Nose Radius
S	Surface Area, State Inequality Constraint
T	Thrust, Absolute Temperature
t	Time
V	Velocity
W	Weight
w	Jet Velocity
X	Down Range
α	Angle-of-Attack
β	Direction Angle of the Resultant Aerodynamic Force, $\tan\beta = L/D$
γ	Flight-Path-Angle, Ratio of Specific Heats
η	Efficiency
θ	Thrust Pitch Angle
μ	Gravitational Constant, Lagrange Multiplier
π	Linear Throttle
Subscripts	
a	Ambient
c	Combustor
KE	Kinetic Energy
R	Pressure Recovery
t	Stagnation Condition
0	Standard, Entry

SUMMARY OF WORK COMPLETED

The first step in our approach to developing guidance laws for a horizontal take-off, air-breathing single-stage-to-orbit vehicle is to characterize the minimum-fuel ascent trajectories. We have developed the capability to generate constrained, minimum-fuel ascent trajectories for a single-stage-to-orbit vehicle. A key component of this capability is the general purpose trajectory optimization program OTIS, developed by the Boeing Company for the Air Force. The pre-production version, OTIS 0.96, has been installed and run on a Convex C-1 at Princeton University. A more recent version, OTIS 1.2, is to be installed in September 1989. We have developed supporting software for generating initial guesses. By employing a direct solution method, state inequality constraints, inherent features of the ascent problem, can be routinely handled without resorting to reduced-order approximations for the vehicle point-mass dynamics.

A propulsion model has been developed covering the entire flight envelope of a single-stage-to-orbit vehicle. Three separate propulsion modes, corresponding to an after-burning turbojet, a ramjet and a scramjet, are used in the air-breathing propulsion phase. For each mode, propulsion performance is modeled using a simple one-dimensional flow analysis. By varying the propulsion model parameters over a reasonable range, one obtains a family of propulsion systems exhibiting certain salient propulsion characteristics covering the range of anticipated propulsion system behavior. A variable thrust rocket engine is implemented for orbit insertion and flight in the upper regions of the atmosphere.

The GHAME aerodynamic model of a hypersonic air-breathing single-stage-to-orbit vehicle has been obtained and implemented. Note that, though the present aerodynamic and propulsion models provide a reasonable starting point for our investigations, other models can be readily implemented.

Preliminary results pertaining to the effects of variations in acceleration constraints, available thrust level and fuel specific impulse on the shape of the minimum-fuel ascent trajectories have been obtained. The results show that, if the air-breathing engines are sized for acceleration to orbital velocity, it is the acceleration constraint rather than the dynamic pressure constraint that is active during ascent. Realistic acceleration constraints can be accommodated by proper adjustment of the throttle and angle of attack with only minor mass penalties. The acceleration constraint is accommodated by increasing the angle of attack to raise the flight path during potentially high acceleration periods and throttling back when the acceleration limit is reached. There are finite trajectory segments on the acceleration boundary. The response to decreasing the level of available thrust is that the vehicle flies uniformly at lower altitude. The flight time is increased, as is the fuel consumption. Changing the I_{sp} has little effect on the optimal trajectory and controls, but does increase the fuel consumption as expected.

1. INTRODUCTION

Horizontal take-off, single-stage vehicles, using air-breathing as well as rocket propulsion, may offer a more economical means of transporting payloads to orbit. The anticipated advantages are the operational flexibility of horizontal take-off, the operational simplicity of a single-stage, and the propellant mass reduction that results from using air-breathing engines. The ultimate objective is to rely completely on the air-breathing engines to accelerate to orbital speed. Effective use of air-breathing propulsion over the entire supersonic and hypersonic speed range requires a ramjet with both a subsonic-combustion mode and a supersonic-combustion mode. To accelerate during the subsonic and transonic phases some additional propulsion mode(s) is necessary. Further discussion of the propulsion system development can be found in [1]. The effective use of air-breathing engines leads to lower altitude ascent trajectories as compared to those of the Space Shuttles. Higher dynamic pressure, higher surface temperatures, and higher acceleration loads result.

A number of studies have been conducted to determine the performance potential of an air-breathing SSTO vehicle. The study by Schoettle [2] provides useful background for our work. Schoettle compared rocket versus combined rocket and ramjet/scramjet performance and concluded that the use of a ramjet engine(s) allows substantial propellant savings, but is heavily penalized by the added weight of the ramjet engine and the structural reinforcements required to accommodate the higher dynamic pressures. The maximum payload delivery trajectory involved dynamic pressures of up to 5850 psf. Only by accommodating dynamic pressures up to at least 1044 psf could a payload delivery advantage over a rocket driven vehicle be realized. As a point of reference, the Space Shuttles do not experience dynamic pressures above 650 psf during their ascent. The payload mass versus peak dynamic pressure curve had a steep slope up to 1566 psf, at which point the payload mass was 80% of the maximum achievable value. Between 1566 psf and 5850 psf, the slope was small and relatively constant. The results of this study by Schoettle and other similar studies offer incentive for continuing research towards the development of an air-breathing SSTO vehicle.

Our objective is to develop guidance logic for a horizontal take-off, air-breathing SSTO vehicle. As a first step, we aim to characterize the minimum-fuel trajectories that an air-breathing SSTO vehicle should ideally fly to achieve maximum performance. Because the optimal trajectory characteristics are critically dependent on the propulsion system and aerodynamic models one adopts, and because there is significant uncertainty as to what these models should be, we will parameterize our ignorance as much as possible, so as to explore the range of possibilities and determine the sensitivities to various features of the models. We will also explore the effects of dynamic pressure, heating, and acceleration constraints on the character of the optimal trajectories. Our guidance approach will then follow naturally from an understanding of the ideal optimal trajectories and controls. That is, the characteristics and appropriate approximations on which to base the guidance scheme will be inferred from the results.

In this report, we lay the groundwork for our characterization of minimum-fuel trajectories for an air-breathing SSTO vehicle. The problem formulation is given. The propulsion system and aerodynamic models are discussed. The solution approach is outlined. And some preliminary results are presented.

2. PROBLEM FORMULATION

In all its generality, the determination of an ascent trajectory, let alone an optimal one, for any launch vehicle constitutes an elaborate problem in itself. With the added complexity of sustained flight in the atmosphere for an extended period of time, inherent to an air-breathing SSTO vehicle, the problem becomes even more formidable. The purpose of this research however, is to obtain a *characterization* of minimum-fuel ascent trajectories. The optimal trajectory characteristics will provide the basis for the subsequent development of a guidance scheme. Therefore, the introduction of some simplifying assumptions which would reduce the overall complexity of the ascent problem without significantly affecting its character is justified.

First, the Earth is assumed to be modeled as a homogeneous sphere. Neglecting the oblateness and inhomogeneity of the Earth implies a central gravity field and allows us to use the simple inverse square law ($g = \mu/r^2$) for the gravitational acceleration.

Second, the Earth is assumed to be non-rotating. This simplification is acceptable considering the very small accelerations experienced due to the Coriolis force. Furthermore, if this force was included the orientation of the ascent trajectory with respect to the Earth rotational axis would come into play, complicating a general trajectory characterization.

Third, the atmosphere is taken to be stationary and in what follows the use of a standard atmosphere providing ambient conditions as a function of altitude only has been assumed.

2.1 Equations of Motion

At this stage we are not considering ascent from a specific launch site to a specific target orbit, but the simpler problem of ascending to a generic low Earth orbit. Intuitively, the minimum-fuel ascent trajectory for this case will not exhibit out-of-plane motion, that is, the ascent trajectory will be confined to a great circle plane and the heading is fixed. Imposing this restriction a priori eliminates the bank angle as a control variable, simplifying the control problem even further. Subsequent work dealing with specific launch site-target orbit pairings will need to take out-of-plane motion into consideration. With this additional simplification and the usual no-slip condition, the dynamic equations describing the motion of the vehicle (or more precise the motion of the center of mass of the vehicle) are [3,4]

$$\frac{dV}{dt} = \frac{T \cos(\theta + \alpha) - D}{m} - g \sin \gamma \quad (1)$$

$$\frac{d\gamma}{dt} = \frac{L + T \sin(\theta + \alpha)}{mV} + \left(\frac{V}{r} - \frac{g}{V} \right) \cos \gamma \quad (2)$$

$$\frac{dr}{dt} = V \sin \gamma \quad (3)$$

$$\frac{dX}{dt} = V \frac{R}{r} \cos \gamma \quad (4)$$

$$\frac{dm}{dt} = - \frac{T}{g_0 I_{sp}} \quad (5)$$

where R is the radius of the Earth and $g_0 = \mu/R^2$. Observe that the direction of the thrust is fixed with respect to the body axes and lies in the vehicle's plane of symmetry. The line of

thrust is offset with a fixed thrust pitch angle θ with respect to the line of zero angle-of-attack. The aerodynamic forces are described by

$$L = C_L q S_{ref} \quad D = C_D q S_{ref} \quad (6)$$

where the lift coefficient (C_L) and the drag coefficient (C_D) are functions of the angle-of-attack (α) and Mach number (M), q is the dynamic pressure and S_{ref} is a reference area. The propulsive force is given most generally by

$$T = \sum_k \pi_k T_{max_k}(M, p_a, T_a, \alpha) \quad (7a)$$

or, equivalently in a standard atmosphere (e.g. the U.S. Standard Atmosphere, 1976 [5]) where the ambient pressure and temperature are functions of the altitude ($h = r - R$) only, by

$$T = \sum_k \pi_k T_{max_k}(M, h, \alpha) \quad (7b)$$

where π_k is a continuous linear throttle factor ranging from zero to one. The thrust dependence on α reflects the influence of incidence on the engine intake performance. The index k allows for more than one particular propulsion mode to be effective at the same time: for example, the use of a throttleable rocket along with a scramjet in the higher regions of the atmosphere.

Likewise, the specific impulse (I_{sp}) is a function of Mach number and either the ambient conditions or the altitude in a standard atmosphere

$$I_{sp_k} = I_{sp_k}(M, p_a, T_a, \alpha) \quad I_{sp_k} = I_{sp_k}(M, h, \alpha) \quad (8)$$

The common assumption is made here that the value of the I_{sp} is not affected by throttling of the engine. This assumption is not always justified and the I_{sp} can depend in a nonlinear fashion on the throttle setting. However, determining I_{sp} as a function of the linear throttle π involves the non-trivial inversion of the propulsion model and seems unwarranted at this stage.

The vehicle dynamics are thus controlled by the angle-of-attack α and the set of linear throttles π_k .

2.2 Initial and Final Conditions

Ideally one would like to consider the ascent from release of the brakes at the beginning of the runway, to insertion into low Earth orbit (LEO). In practice however the execution of a minimum fuel ascent will be restricted by safety and operational considerations to commence after take-off and initial-climb out. Additionally, the acceleration to supersonic speeds employing a turbojet-like mode of propulsion is well understood and this phase of the ascent to orbit accounts for only a small portion of the total fuel consumption. Hence our work has been focused on the high-speed phase of the ascent.

Similarly, the final insertion into low Earth orbit using a rocket orbital maneuvering system is well understood and actual determination of the orbit insertion might be computationally intensive due to extreme sensitivity of various orbital parameters to the insertion parameters. Instead, acceleration to circular speed at the edge of the sensible atmosphere is used to benchmark the various optimal ascent trajectories.

Subsequent work may include a more detailed look at the coupling between the trunk ascent trajectory and the initial climb-out and orbital insertion phase respectively.

2.3 Performance Index

Since this work is concerned with minimum-fuel ascent to orbit the obvious performance index to be minimized is the fuel expenditure. For a vehicle with a fixed gross take-off weight this is equivalent to maximizing final weight. The ultimate purpose of the air-breathing ascent is to maximize payload/fuel mass fraction. To this end one should make the gross take-off weight a design (i.e. free) variable. This has not been taken up here since, if done properly, it would amount to a full-fledged design study. Our study is limited to the case of a fixed gross take-off weight and the minimum-fuel ascent trajectories are obtained by formally maximizing the final mass.

2.4 State and Control Constraints

Vehicle and crew considerations dictate certain constraints that must be placed on the states and/or controls. The throttle settings must take on values between 0 and 1. The angle of attack must take on values between α_{\min} and α_{\max} . The value of α_{\max} corresponds to either the stall boundary or a propulsion system dictated boundary. The minimum angle of attack is dictated by the propulsion system characteristics or the limits of our aerodynamic data. α_{\min} is typically some small negative angle.

We consider two state and control inequality constraints that place limits on the axial and normal acceleration loads

$$C_1 = | 1/m (\pi T_{\max} - (L^2 + D^2)^{1/2} \cos(\alpha + \beta)) | - G_{\text{axial}} \leq 0 \quad (9)$$

$$C_2 = | 1/m ((L^2 + D^2)^{1/2} \sin(\alpha + \beta)) | - G_{\text{normal}} \leq 0 \quad (10)$$

where $\tan\beta = L/D$ and G_{axial} and G_{normal} are the imposed acceleration limits. A less specific option for constraining the acceleration load is to limit the total acceleration load

$$C = 1/m (\pi^2 T_{\max}^2 + L^2 + D^2 + 2\pi T_{\max}(L\sin\alpha - D\cos\alpha))^{1/2} - G_{\text{total}} \leq 0$$

We also consider the two first-order state inequality constraints that place limits on the heating rate and dynamic pressure

$$S_1 = K \rho^{1/2} V^3 - Q_{\max} \leq 0 \quad (11)$$

$$S_2 = \frac{1}{2} \rho^{1/2} V^2 - q_{\max} \leq 0 \quad (12)$$

Clearly, the set of constraints could be greatly expanded, but this would require specific vehicle knowledge. In order to keep our study generic and not over-complicate the computations, we will not go beyond the above set of constraints.

2.5 Optimality Conditions

Even though we will be employing a direct method of solution, some insight into the characteristics of the minimum-fuel trajectories and controls may be obtained from deriving the optimality conditions that would form the basis of an indirect method of solution.

The Hamiltonian for the constrained minimum-fuel ascent problem is

$$H = \mathbf{p}_r \cdot \mathbf{V} + \mathbf{p}_v \cdot \left(\frac{1}{m} (\mathbf{T} + \mathbf{A}) + \mathbf{g}(\mathbf{r}) \right) - p_m \frac{T}{g_0 I_{sp}} + \sum_{i=1}^4 \mu_i C_i \quad (13)$$

where μ_i , $i = 1-4$, are Lagrange multipliers

$$\mu_i \leq 0 \quad \text{for} \quad C_i = 0$$

$$\mu_i = 0 \quad \text{for} \quad C_i < 0$$

and

$$C_3 = \frac{dS_1}{dt}$$

$$C_4 = \frac{dS_2}{dt}$$

The equations for the adjoint variables are

$$\frac{d\mathbf{p}_r}{dt} = - \frac{\partial H}{\partial \mathbf{r}} \quad (14)$$

$$\frac{d\mathbf{p}_v}{dt} = - \frac{\partial H}{\partial \mathbf{V}} \quad (15)$$

$$\frac{dp_m}{dt} = - \frac{\partial H}{\partial m} \quad (16)$$

If the optimal trajectory contains an arc that is on the boundary of one of the first-order state constraints, conditions of the form [6]

$$S_i(\mathbf{r}, \mathbf{V}) = 0 \quad (17)$$

$$\mathbf{p}_r^T(t_k^-) = \mathbf{p}_r^T(t_k^+) + \lambda_r \frac{\partial S_i}{\partial \mathbf{r}}(t_k) \quad (18)$$

$$\mathbf{p}_v^T(t_k^-) = \mathbf{p}_v^T(t_k^+) + \lambda_v \frac{\partial S_i}{\partial \mathbf{V}}(t_k) \quad (19)$$

$$p_m(t_k^-) = p_m(t_k^+) \quad (20)$$

$$H(t_k^-) = H(t_k^+) \quad (21)$$

apply at the entry or exit from the boundary arc, where t_k is the entry or exit time and λ_r and λ_v are scalar Lagrange multipliers. The entry and exit points may or may not be corners, i.e., places where some or all of the controls are discontinuous.

For flight away from the constraint boundaries, the optimal controls are as follows. Based on the Maximum Principle, the values of the controls at each point along the optimal trajectory

should maximize H. Taking the partial derivatives of H with respect to the controls and expressing the result in terms of the state variables used in Eqs. (1)-(3) and (5) and the corresponding adjoint variables, we obtain

$$\frac{\partial H}{\partial \pi} = \frac{T_{\max}}{m} \left(p_v \cos(\theta + \alpha) + p_\gamma \frac{\sin(\theta + \alpha)}{V} - p_m \frac{m}{g_s I_{sp}} \right) \quad (22)$$

$$\frac{\partial H}{\partial \alpha} = p_\gamma \left(\frac{T}{mV} \cos(\theta + \alpha) + \frac{qS}{mV} \frac{\partial C_L}{\partial \alpha} \right) - p_v \left(\frac{T}{m} \sin(\theta + \alpha) + \frac{qS}{m} \frac{\partial C_D}{\partial \alpha} \right) \quad (23)$$

Since the control π appears linearly in H and $\partial H/\partial \pi$ is its coefficient, H is maximized by choosing π according to the rule

$$\begin{aligned} \pi &= 0 & \text{if} & \quad \partial H/\partial \pi < 0 \\ \pi &= 1 & \text{if} & \quad \partial H/\partial \pi > 0 \end{aligned} \quad (24)$$

If $\partial H/\partial \pi = 0$ over a finite interval of time, the control is singular and must be determined from higher order conditions. We will show below that the singular case can be ruled out. The control α is bounded from above and below. H may be maximized by α_{\min} , α_{\max} , or an interior value of α that satisfies the implicit equation

$$\frac{p_\gamma}{V p_v} = \frac{\frac{T}{m} \sin(\theta + \alpha) + \frac{qS}{m} \frac{\partial C_D}{\partial \alpha}}{\frac{T}{m} \cos(\theta + \alpha) + \frac{qS}{m} \frac{\partial C_L}{\partial \alpha}} \quad (25)$$

The Hessian of H with respect to the controls, denoted by H_{uu} , has components

$$\frac{\partial^2 H}{\partial \pi^2} = 0 \quad (26)$$

$$\frac{\partial^2 H}{\partial \alpha \partial \pi} = \frac{\partial^2 H}{\partial \pi \partial \alpha} = \frac{T_{\max}}{m} \left(-p_v \sin(\theta + \alpha) + p_\gamma \frac{\cos(\theta + \alpha)}{V} \right) \quad (27)$$

$$\frac{\partial^2 H}{\partial \alpha^2} = -\frac{\pi T_{\max}}{m} \left(p_v \cos(\theta + \alpha) + \frac{p_\gamma}{V} \sin(\theta + \alpha) \right) + \frac{qS}{m} \left(\frac{p_\gamma}{V} \frac{\partial^2 C_L}{\partial \alpha^2} - p_v \frac{\partial^2 C_D}{\partial \alpha^2} \right) \quad (28)$$

If an interior value of α satisfying Eq. (25) maximizes H, the second partial given in Eq. (28) should be less than or equal to zero; if it is equal to zero, higher derivatives with respect to α would have to be checked.

In order to determine whether a singular thrust arc can be optimal, we examine the determinant of H_{uu} . From Eqs. (26)-(28), it follows that

$$\det(H_{uu}) = - \left(\frac{T_{\max}}{m} \right)^2 \left(- p_v \sin(\theta + \alpha) + p_\gamma \frac{\cos(\theta + \alpha)}{V} \right)^2 \quad (29)$$

Thus $\det(H_{uu}) \leq 0$. If $\det(H_{uu}) < 0$, H_{uu} is indefinite and the singular arc is not optimal. If $\det(H_{uu}) = 0$, then the singular arc may be optimal and additional conditions would have to be checked. The first factor on the right-hand-side of Eq. (29) is never zero based on physical reasoning; the second factor is zero only if $p_v = p_\gamma = 0$ or

$$\tan \alpha = \frac{p_\gamma}{V p_v} \quad (30)$$

The first condition implies that $p_r = p_m = 0$ as well and is inconsistent with an optimal solution. Referring to Eq. (25), the second condition can only be satisfied in the limit as the density ρ (and hence q) goes to zero, i.e., outside the atmosphere. Consequently, we conclude that singular thrust arcs are not optimal during the ascent through the atmosphere. Corban, Calise, and Flandro[28] reached the same solution for a reduced-order model of the point mass dynamics.

Transversality conditions, integrals of the motion, and the optimal controls for flight on the constraint boundaries will not be developed here, since no further insight is expected. We only remark that intermediate values of throttle are possible along constraint boundaries. The results to be described later show that indeed intermediate values of throttle are used to fly along the boundary of the acceleration constraint.

In the above development, the issue of choosing the optimal propulsion mode has not been addressed. Accounting for the existence of different propulsion modes, we rewrite the Hamiltonian as

$$\begin{aligned} H_{\text{reduced}} &= \sum_{i=1}^k \left(\frac{p_v}{m} \cos(\theta + \alpha) + \frac{p_\gamma}{mV} \sin(\theta + \alpha) - \frac{p_m}{g_0(I_{sp})_i} \right) \pi_i(T_{\max})_i \\ &= [p_v \quad p_\gamma \quad p_m] \sum_{i=1}^k \begin{pmatrix} \frac{\cos(\theta + \alpha)}{m} \\ \frac{\sin(\theta + \alpha)}{m} \\ -\frac{1}{g_0(I_{sp})_i} \end{pmatrix} \pi_i(T_{\max})_i \end{aligned} \quad (31)$$

where k is the number of propulsion modes and the subscript "reduced" denotes that the terms not involved in determining the optimal throttle setting have been suppressed. In the second line of the equation, the reduced Hamiltonian is expressed in the form of an inner product (actually there are k inner products). At this point in our investigations, we are assuming that only one propulsion mode is active at any given time. The optimal mode is the one associated with the largest of the k inner products. Since the angle of attack appears in these inner products and the k throttle settings appear in the equations for determining the optimal angle of attack, the optimal controls must be determined by simultaneous maximization of the Hamiltonian. At points along the optimal trajectory where there is a switch from one propulsion mode to another, there will in general be corners where there are discontinuities in the time derivatives of the speed and flight path angle.

3. VEHICLE MODELING

The current vehicle configuration is conform a series of NASA reports on a Hypersonic Research Airplane Concept [7-10]. The airframe is expected to be a cross between a flying body and a delta wing with a belly-mounted multi-mode engine. The gross take-off weight of the SSTO vehicle is estimated to be 300,000 lbf of which approximately 60 % is fuel [11]. The overall length of the vehicle is approximately 233.4 ft and its aerodynamic reference area is 6,000 sqft.

Liquid hydrogen is used as fuel over the entire speed range since it allows for the high effective specific impulse that makes air-breathing propulsion a viable option and is suitable for supersonic combustion. Recently, slush hydrogen has been mentioned as an operationally more attractive form of the hydrogen fuel [12].

3.1 The Aerodynamic Characteristics

Currently, there is a dearth of up-to-date aerodynamic data concerning lifting vehicles flying at hypersonic speeds. However, representative values for the lift and drag coefficients covering the entire flight regime of a SSTO vehicle, have been obtained from . The generic hypersonic aerodynamic data therefore contains certain realistic aerodynamic anomalies.

The present study is concerned with guidance for performance, that is, it considers the motion of the vehicle's center of mass. The C_L and C_D values used in this point mass model are the trimmed (equilibrium) values as functions of Mach number and angle-of-attack α ; the rotational dynamics are not accounted for. ones obtained by instantaneous trimming of the vehicle. We currently employ the trim map found in the Generic Hypersonic Aerodynamic Model Example (GHAME) [11] which covers the entire flight regime of a SSTO vehicle. This model is an amalgamation of the characteristics of the space shuttles, the X-24C lifting body and a 70° swept double delta wing configuration. In Figure 1, C_L and C_D are plotted as a functions of Mach number for a selected number of angles-of-attack. These plots are obtained from the original data grid by quadratic interpolation over α for fixed Mach number and subsequent determination of cubic splines for the quadratic coefficients over the Mach number range. Actual numerical calculations however employ local 2-dimensional quintic interpolation applied to the original data grid.

3.2 The Propulsion System

The aero-engine for an air-breathing SSTO vehicle comprises several distinct propulsion modes, each suited to operate over a specific speed range. Our present propulsion model consists of an afterburning single-flow turbojet, a ramjet and a scramjet. The model is designed to provide maximum specific thrust and the corresponding fuel specific impulse. The respective modes are analyzed using simple one-dimensional flow analysis for perfect gases, employing appropriately constant efficiencies [13-18].

A simple turbojet model has been developed for completeness and may or may not accurately represent the actual low speed propulsion mode; there is still much uncertainty about the kind of propulsive device to be used for take-off and climb-out.

The emphasis of our work has been on the high-speed phase of the ascent after initial acceleration to supersonic speeds. At these speeds a ramjet with either subsonic or supersonic combustion is most suitable. Though we do not want to concern ourselves with the mechanical particulars of such an engine, one may visualize an integrated device where upstream transfer of the combustion process effects a switch from a ramjet with conventional subsonic combustion to a ramjet with supersonic combustion: a scramjet. A brief description of the respective ramjet propulsion modes is presented in what follows, for more detail the reader is referred to the Appendix.

The advantage of the present propulsion model based on fundamental thermodynamic relations is that it allows us to obtain different propulsion characteristics by changing specific engine efficiencies and parameters.

At high speeds the entire vehicle becomes a flying engine, its forebody functioning as a compression surface and its trailing edge as an expansion surface. The inlet and exit characteristics of the propulsion device can therefore not be modeled accurately by a simplified analysis or existing design methods (e.g. additive drag, intake efficiency and nozzle losses). However, it is reasonable to expect that the variable geometry inlet is designed to reduce the effect of inlet spillage on the performance and that the intake is always matched to the engine. Hence, for the moment, additive drag has been neglected. Similarly, the 3D-nozzle is represented only by its thermodynamic workings. A simple estimate for the internal friction of the engine has been incorporated.

The effect of incidence on the engine performance with belly-mounted engine pods is twofold [19]. First, increased incidence leads to a larger mass capture by forebody-intake system and thus will enhance the thrust. On the other hand increased incidence produces a stronger bow shock and will decrease the efficiency of the intake process thus decreasing the thrust. At very high incidence the loss in efficiency will outweigh the gain in massflow since the latter has an upperbound dictated by the engine size. The two opposite trends will therefore most likely result in either an immediate roll-off in thrust or an initial increase followed by a roll-off.

3.1.1 The Ramjet. The airflow is diffused adiabatically to subsonic speeds with constant kinetic efficiency. The airflow enters the combustor at constant Mach number. Combustion takes place with constant burning efficiency and a fixed drop in stagnation pressure. The amount of fuel is determined by the maximum combustor exit temperature.

Next the airflow is accelerated again to supersonic speeds through a continuously adjustable convergent-divergent nozzle. Ideally the flow should expand to ambient pressure for maximum performance, however, the nozzle's expansion ratio is limited by the maximum size of the exit area.

The specific thrust and specific impulse determined from this model for a couple of altitudes in the 1976 U.S. Standard Atmosphere are presented in Figure 2, for the specific set of ramjet parameter values presented in Table 1. Towards Mach = 7 the combustor stagnation entry temperature approaches the fixed combustor stagnation exit temperature, resulting in a rapid decline in thrust and a steep drop in specific impulse. Observe furthermore the relative insensitivity of the specific impulse as a function of Mach number to changes in altitude as opposed to the thrust.

3.1.2 The Scramjet. In this propulsion mode the airflow is diffused to supersonic speeds with constant process efficiency. Swithenbank [14] recommends a diffusion ratio of 3.0 for optimal specific impulse, hence the intake delivery Mach number is taken to be one third of the flight Mach number.

In our original scramjet model, the supersonic combustion takes place at constant combustor cross section area. An approximate optimal fuel-to-air ratio as a function of flight Mach number is obtained from [14]. The fuel mixture is weaker than stoichiometric at flight speeds below $M = 10$ and richer at speeds approaching circular velocity.

$$\begin{aligned} m_{\text{fuel}} / m_{\text{air}} &= 0.003 \times M & M < 12.5 \\ m_{\text{fuel}} / m_{\text{air}} &= 0.0375 & M \geq 12.5 \end{aligned} \tag{32}$$

In case this fuel-to-air ratio leads to thermal choking the amount of fuel is reduced to the critical amount, for which the flow reaches marginal choking conditions at the combustor exit. Thermal choking occurs for flight Mach numbers less than approximately 10.7. This resulted in an inadequate level of thrust in the lower Mach number range of $M = 4$ to 6. The range where, according to reports [20], the scramjet is expected to kick in. In our revised model, the supersonic combustion can take place in a variable cross section area burner. The additional parameter also allows for the limiting case of constant pressure combustion, which is thought to be more conducive to the combustion process.

Since the flow is supersonic, the nozzle consists of a divergent section only. The expansion ratio is again fixed by the size of the exit area. The nozzle efficiency as expressed by the value of the velocity coefficient C_v turns out to have a significant effect on the form of the propulsion characteristic. Over a relatively narrow range of C_v values the specific thrust characteristic is found to change from monotonically increasing with Mach number to rolling off at high Mach numbers. Since there is still much uncertainty about the true behavior of the scramjet at very high speeds, it is important to determine the effect of this variation in thrust character on the make-up of the ascent trajectory.

The specific thrust and specific impulse determined from this model for a couple of altitudes in the U.S. Standard Atmosphere, 1976 are presented in Figure 3 for the original model and the specific values for the scramjet parameters presented in Table 2. Figure 4 shows the characteristics of the revised model at two different values of the nozzle velocity coefficient C_v , with the specific parameter values presented in Table 3.

The airflow through the combustor is thermally choked below $Mach = 10.7$ in the original model, this shows up as a corner in the thrust and I_{sp} graphs. With the revised model this corner indicates the transition from a variable cross-sectional area combustor to a constant cross-sectional area one. The second corner in both graphs is related to the slope discontinuity in the fuel-to-air ratio at $M = 12.5$. The rise in the specific impulse of the scramjet at high Mach numbers is caused by the specific impulse contribution due to the kinetic energy of the fuel. This becomes a significant contribution at high speeds. Furthermore, the revised model is seen to predict I_{sp} levels of 3200 to 4000 seconds, consistent with those cited in [21].

3.2.3 The Rocket. In order to be able to maneuver in space the SSTO vehicle must have a rocket engine. Depending on the performance of the scramjet at high speeds and high altitudes there might also be a need to employ a rocket before exiting the atmosphere.

The RL-10 rocket engine for the Centaur upper stage is suggested by Calise et al [22] to be representative of a rocket engine to be installed in a SSTO vehicle. It is rated at 15,000 lbf thrust and a I_{sp} of 444 sec at 200,000 ft [23]. Back pressure will be taken into account employing an exhaust area of 11.5 sqft.

4. SOLUTION APPROACH

Flight path optimization, based on a calculus of variations formulation, entails the solution of a nonlinear two point boundary value problem [6]. This is a difficult task which is exacerbated when state and control inequality constraints are imposed. Because of the critical role of state and control inequality constraints in the present flight path optimization problem, we sought an optimization algorithm that could readily accommodate such constraints. We are currently using a computer program entitled Optimal Trajectories by Implicit Simulation (OTIS) [24], installed on a Convex C-1. Thus far it has served us well.

The approach, on which OTIS is based, is to formulate the optimal control problem as a nonlinear programming problem using implicit integration of the trajectory by a collocation method. The states along the trajectory as well as the controls are represented by cubic splines. The collection of breakpoints (or nodes) of the cubic segments constitutes a discretization of the trajectory. By adjoining the defects of the collocation at the midpoint between successive nodes to the original performance index, one obtains an augmented performance index, subject to the original boundary conditions and constraints evaluated at the nodes and the midpoints. In this manner the original optimal control problem is stated in the form of a constrained nonlinear programming problem [25]. The independent variables are the states and the controls at the nodes plus the length of the time interval. To solve such a programming problem a host of methods is available, see [26]. The present version of OTIS employs the NPSOL 2.1 package [27].

OTIS needs an initial estimate, preferably a feasible trajectory. We obtained our original feasible trajectory by piecing together segments of flight at constant dynamic pressure, constant altitude and constant throttle setting. The trajectories of previous runs were used for subsequent initial estimates.

Observe that the augmented performance index is only locally minimized and depends on the initial estimate, the scaling of variables and constraints and the specific node distribution. In order to accept any result as a locally optimal solution, one needs to verify relative insensitivity to the node distribution. The total number of nodes employed currently is 65, which is pushing the capacity of our machine.

5. RESULTS

We present some preliminary results which only begin our characterization of the minimum-fuel ascent trajectories. The conditions at the end of the initial climb-out and acceleration phase, the phase in which the turbojet propulsion mode is assumed to be used, are estimated to be Mach 2 in speed, 1,000 psf in dynamic pressure, and zero degrees in flight path angle. The weight of the vehicle is estimated to be reduced to 290,000 lbf at the end of the climb-out, from 300,000 lbf gross take-off weight. These quantities determine the initial conditions for the minimum-fuel ascents (see Table 4a). The final conditions correspond to a circular orbit at the edge of the sensible atmosphere, which is thought to occur at 259,000 ft, leading to a final speed and flight-path-angle of 25,777 fps and 0° respectively (see Table 4b).

In order not to limit, a priori the vehicle's flight envelope, the engines are sized so that orbital insertion using air-breathing propulsion only is feasible. With insertion into a 50 nm by 100 nm transfer orbit as a typical target orbit, a combustor cross-sectional area of 400 ft² was found to provide an adequate level of thrust of 4,000 lbf at the insertion point with the original propulsion model. Together with data mentioned in earlier chapters, this defines the (preliminary) baseline vehicle (see Table 4c). Additionally, the thrust level does not depend on the angle-of-attack, i.e., the sensitivity of thrust with respect to incidence effects has not been considered. The thrust pitch angle is identically zero.

In the numerical computations the angle-of-attack range was restricted to the range of our aerodynamic data (-3° to 21°) and the α rate of change was limited as to require one second to traverse the entire a range. Likewise, the throttle rate of change was restricted to be less than 20 %/sec, precluding the occurrence of bang-bang and chattering controls.

5.1 Effect of Acceleration Constraints

The baseline model with engines sized for orbital insertion and capable of generating high levels of thrust in the lower regions of the atmosphere will consequently be able to accelerate very rapidly. However, as mentioned in section 2.4, there are limits to the allowable level of sustained acceleration. It is therefore of interest to assess the effect of the magnitude of the acceleration limit on the character of the ascent trajectory and to evaluate the relative penalty incurred using a more stringent limit. Three acceleration limits were implemented varying from 5g's to 3g's.

The results in Table 5a show that, as expected, the performance as measured by the value of the final mass diminishes as the acceleration constraint becomes more stringent, while the time of ascent increases. The penalty one has to pay for the convenience of ascending to orbit at 3g's as opposed to 5g's is however a meager 1,000 lbf.

Additionally, it is interesting that the Mach number and altitude at which the switch is made from ramjet to scramjet shows little sensitivity to the value of a_{max} . This is also evident from Figure 5. Referring back to Figures 1 and 2, note that the switch occurs in the Mach number range where the I_{sp} of the ramjet starts falling off but is still superior to the scramjet I_{sp} which is near its maximum value. The bottom curve in Figure 5 represents a constant dynamic pressure of 1,500 psf. It shows that along all three ascent trajectories the dynamic pressure is less than 1,500 psf, although no dynamic pressure constraint has been imposed.

Figures 6a and b show another general characteristic: the vehicle uses full throttle unless it has reached the acceleration constraint, in which case it throttles back in order to follow the constraint. The same figures also illustrate the switch between propulsion modes. At both sides of the switch the propulsion system is at full throttle. The switch occurs apparently when the drop in I_{sp} in going from ramjet to scramjet is outweighed by the higher scramjet thrust.

Figure 7 presents the other control variable, the angle-of-attack. The character of the angle-of-attack vs. Mach number curve is similar for the three acceleration limits. The

angle-of-attack is generally higher, the lower the acceleration limit. Higher angle-of-attack produces higher lift and consequently the higher altitude flight path seen in Figure 5.

5.2 Effect of Available Thrust Level

The combustor cross-sectional area for the baseline model roughly corresponds to a frontal intake area of 670 sqft [15]. The intake to reference area ratio of 0.112 contrasts sharply with the area ratio of 0.0195 for the Hypersonic Research Airplane Concept of [7-10]. Although it should be observed that the latter is a hypersonic cruise vehicle and not a SSTO boost vehicle, the discrepancy points out that the actual engine size could be determined by factors other than air-breathing orbital insertion capability. Therefore, the available thrust level may not be quite as high as assumed for the baseline model. Using the 300 sqft frontal intake area suggested in [11], a combustor cross-sectional area of 180 sqft is obtained. The effect of the overall thrust level on the minimum-fuel ascent is estimated, evaluating three engine sizes varying from the baseline 400 sqft combustor to a 180 sqft one. A 3g's acceleration limit is employed in all three cases.

The results in Table 5b show a 33% increase in final time, resulting in increased fuel consumption. The propulsion mode switching still occurs in the same Mach number range, while the linear throttle exhibits the same kind of generic behavior as noted in the previous section, see Figure 6c. However, as illustrated by Figure 8, the vehicle with the reduced engine size shows an overall tendency to fly lower at higher levels of dynamic pressure. This tendency most likely stems from the fact that thrust is proportional to dynamic pressure.

5.3 Effect of Fuel Specific Impulse

Presently, there is much uncertainty concerning the performance of the sub/supersonic combustion ramjet. Therefore, it is of interest to determine what effect a drop in overall engine performance, as expressed by the fuel specific impulse, has on the character of the minimum-fuel ascent. Employing the baseline model and again a 3g acceleration limit, three trajectories have been determined with I_{sp} levels ranging from 100% to 60% of our baseline values.

The results presented in Table 5c indicate a modest sensitivity to the engine performance as far as trajectory make-up is concerned, with a slight increase in altitude at lower I_{sp} (see Figure 9), where lower ambient temperatures lead to improved performance. In contrast, the effect on the final mass is very profound as was to be expected. The linear throttle still shows the same generic behavior, effectively functioning as a direct acceleration control.

6. CONCLUSIONS AND WORK IN PROGRESS

We have developed the capability to generate constrained, minimum-fuel ascent trajectories for a single-stage-to-orbit vehicle. By employing a direct solution method, state inequality constraints, inherent features of the ascent problem, can be routinely handled without resorting to reduced-order approximations for the vehicle point-mass dynamics. A model, based on one-dimensional flow analysis, has been developed for a multi-mode propulsion system capable of turbojet, ramjet, scramjet, and rocket performance. The free parameters of the propulsion model can be adjusted to obtain a range of performance. Aerodynamic parameters have been obtained from the GHAME. The developed capability enables us to characterize the minimum-fuel ascent trajectories. Subsequent guidance law development will be based on the results of the characterization.

Results pertaining to the effects of variations in acceleration constraints, available thrust level and fuel specific impulse on the shape of the minimum-fuel ascent trajectories have been obtained. The results show that, if the airbreathing engines are sized for acceleration to orbital velocity, it is the acceleration constraint rather than the dynamic pressure constraint that is active during ascent. Realistic acceleration constraints can be accommodated by proper adjustment of the throttle and angle of attack with only minor mass penalties. The acceleration constraint is accommodated by increasing the angle of attack to raise the flight path during potentially high acceleration periods and throttling back when the acceleration limit is reached. There are finite trajectory segments on the acceleration boundary. The response to decreasing the level of available thrust is that the vehicle flies uniformly at lower altitude; the flight time is increased, as is the fuel consumption. Changing the I_{sp} has little effect on the optimal trajectory and controls, but does increase the fuel consumption as expected.

Our initial minimum-fuel trajectory results showing acceleration to be the limiting constraint are inconsistent with those of other investigators [2,22,28] who have found dynamic pressure to be the limiting constraint. Since the work reported in Chapter 5 was completed, a revised scramjet model has been developed. This revised model allows us to investigate the effect of thrust roll-off at high speeds on the characteristics of the minimum-fuel ascent. We are currently computing minimum-fuel trajectories, for which the rocket engine is allowed to augment the air-breathing thrust capability during the ascent. With this approach, we avoid having to size the air-breathing engines for acceleration to orbital velocity. As discussed in Section 5.2, lower air-breathing engine thrust levels lead to higher dynamic pressures. Thus we should obtain results that are more in line with those of other investigators.

We also intend to investigate the effects of making the thrust level dependent on angle-of-attack or the thrust pitch angle. Scaling the thrust by a quadratic function of angle of attack will allow us to investigate several types of thrust variation by using different values of the coefficients in the quadratic function. For the proposed type of air-breathing SSTO vehicles where the fore- and aftbody of the vehicle constitute integral parts of the propulsion system, the direction of thrust will vary with flight conditions. We plan to develop a means simulating this feature and then to determine the consequences.

Much useful insight into the characteristics of the minimum-fuel ascent trajectories has been gained using reduced-order models [22,28]. An important question that needs to be answered is: How well do the optimal trajectories for the reduced-order models approximate the optimal trajectories for the full-order model? We intend to answer this question and are proceeding to develop software to generate reduced-order solutions.

Finally, we plan to spend much of the next year on initial guidance law development.

REFERENCES

- [1] Donaldson, P., "Developing Air-Breathers", *Space*, Vol. 4, No. 4, July-Aug. 1988.
- [2] Schoettle, U.M., "Performance Analysis of Rocket-Ramjet Propelled SSTO Vehicles", 36th Congress of the International Astronautical Federation, Stockholm, Sweden, Oct. 7-15, 1985, IAF-85-133.
- [3] Miele, A., **Flight Mechanics**, Vol.1 Theory of Flight Paths, Addison-Wesley Publishing, 1962.
- [4] Vinh, N. X., Busemann, A., and Culp, R. D., **Hypersonic and Planetary Entry Flight Mechanics**, University of Michigan Press, Ann Arbor, 1980.
- [5] "U.S. Standard Atmosphere, 1976", U.S. Government Printing Office, 1976.
- [6] Bryson, A. E., Jr. and Ho, Y. C., **Applied Optimal Control**, Hemisphere Publishing Corporation, New York, 1975.
- [7] Penland, J.A., Fournier, R.H., and Marcum, Jr., D.C., "Aerodynamic Characteristics of a Hypersonic Research Airplane Concept Having a 70° Swept Double-Delta Wing at Mach Numbers From 1.50 to 2.86", NASA TN D-8065, 1975.
- [8] Dillon, J.L., and Pittman, J.L., "Aerodynamic Characteristics at Mach Numbers From 0.33 to 1.20 of a Wing-Body Design Concept for a Hypersonic Research Airplane", NASA Technical Paper 1044, 1977.
- [9] Dillon, J.L., and Pittman, J.L., "Aerodynamic Characteristics at Mach 6 of a Wing-Body Design Concept for a Hypersonic Research Airplane", NASA Technical Paper 1249, 1978.
- [10] Penland, J.A., Hallissy, J.B., and Dillon, J.L., "Aerodynamic Characteristics of a Hypersonic Research Airplane Concept Having a 70° Swept Double-Delta Wing at Mach Numbers From 0.80 to 1.20, With Summary of Data From 0.20 to 6.0", NASA Technical Paper 1552, 1979.
- [11] Bowers, A.H., and Iliff, K.W., "A Generic Hypersonic Aerodynamic Model Example (GHAME) for Computer Simulation", 1988, Proposed NASA TM.
- [12] *Aviation Week & Space Technology*, June 26, 1989, pg. 37-38.
- [13] Loh, W.H.T. ed., **Jet, Rocket, Nuclear, Ion and Electric Propulsion: Theory and Design**, Springer-Verlag New York Inc. 1968.
- [14] Swithenbank, J., "Hypersonic Air-Breathing Propulsion", *Progress in Aeronautical Sciences*, Vol.8, 1967, pp.229-294.
- [15] Small, W.J., Weidner, J.P., and Johnston, P.J., "Scramjet Nozzle Design and Analysis as Applied to a Highly Integrated Hypersonic Research Airplane", NASA TN D-8334, 1983.
- [16] Kerrebrock, J.L., **Aircraft Engines and Gas Turbines**, The MIT Press, 1977.
- [17] Cohen, H., Rogers, G.F.C., and Saravanamuttoo, H.I.H., **Gas Turbine Theory**, Longman, 1984.
- [18] Whittle, F., **Gas Turbine Aero-Thermodynamics**, Pergamon Press, 1981.
- [19] Hurd, R. "Supersonic Inlets", AGARDograph 102, 1969.
- [20] *Aviation Week & Space Technology*, June 26, 1989, pg. 79.
- [21] *Aviation Week & Space Technology*, July 10, 1989, pg. 11.
- [22] Calise, A.J., Flandro, G.A., and Corban, J.E., "Trajectory Optimization and Guidance Law Development for National Aerospace Plane Applications", Final Report for Period July 1, 1987 to November 30, 1988, NASA CR Number NAG-1-784, 1988.
- [23] "Jane's All the World's Aircraft", J.W.R. Taylor ed., Franklin Watts, 1976.
- [24] Hargraves, C.R., Paris, S.W., and Gailey, J.W., **Optimal Trajectories by Implicit Simulation Manual**, Vol. I-IV, 1988, AFWAL TR-88-3057.

- [25] Hargraves, C.R. and Paris, S.W., "Direct Trajectory Optimization Using Nonlinear Programming and Collocation", *Journal of Guidance, Control and Dynamics*, Vol. 10, No. 4, July-Aug. 1987.
- [26] Gill, P.E., Murray, W., and Wright, M.H., **Practical Optimization**, Academic Press, 1981.
- [27] Gill, P.E., Murray, W., Saunders, M.A., and Wright, M.H., "User's Guide for NPSOL (Version 2.1): A FORTRAN Package for Nonlinear Programming", Technical Report SOL 84-7, Systems Optimization Laboratory, Department of Operations Research, Stanford University, Stanford, CA, September 1984.
- [28] Corban, J. E., Calise, A. J., and Flandro, G. A., "Optimal Guidance and Propulsion Control for Transatmospheric Vehicles," Paper 89-3617, AIAA Guidance, Navigation, and Control Conference, Boston, MA, August 1989.

Table 1 Ramjet Mode Engine Parameters

Intake Kinematic Efficiency	0.94
Combustor Entry Mach Number	0.5
Combustion Efficiency	0.96
Combustor Stagnation Pressure Loss	3 %
Combustor Stagnation Exit Temperature	2500 K
Nozzle Velocity Coefficient	0.97
Nozzle Exit-Combustor Cross Section Area Ratio	6

Table 2 Scramjet Mode Engine Parameters (Original Model)

Intake Process Efficiency	0.93
Diffusion Ratio M_0/M_3	3
Combustion Efficiency	0.96
Nozzle Velocity Coefficient	0.96
Nozzle Exit-Combustor Cross Section Area Ratio	6

Table 3 Scramjet Mode Engine Parameters (Revised Model)

Intake Process Efficiency	0.92
Diffusion Ratio M_0/M_3	3
Combustor Area Change Parameter	$E = 0.0 \quad M \leq 3.0$ $E = (M-3)/7.7 \quad 3.0 \leq M \leq 10.7$ $E = 1.0 \quad M \geq 10.7$
Combustion Efficiency	0.93
Nozzle Velocity Coefficient	0.93/0.91
Nozzle Exit-Combustor Cross Section Area Ratio	6

Table 4a Initial Conditions

Mass	9013.5 slugs
Mach Number	2.0
Dynamic Pressure	1,000 lbf/ft ²

Table 4b Final Conditions

Altitude	259,000 ft
Velocity	25,777 ft/sec
Flight Path Angle	0.0 °

Table 4c Baseline Vehicle Model

Gross Take-Off Weight	300,000 lbf
Reference Area	6,000 ft ²
Combustor Cross Section Area	400 ft ²
Fuel Specific Impulse	100 %

Table 5a Effect of Acceleration Constraint (Baseline Model)

a_{\max} (g)	M_{switch}	h_{switch} (ft)	q_{peak} (lb _f /ft ²)	m_{final} (slugs)	t_{final} (sec)
3.0	6.59	100,987	1,025	5,844	557.1
4.0	6.63	98,902	1,134	5,863	524.7
5.0	6.66	97,373	1,273	5,873	504.5

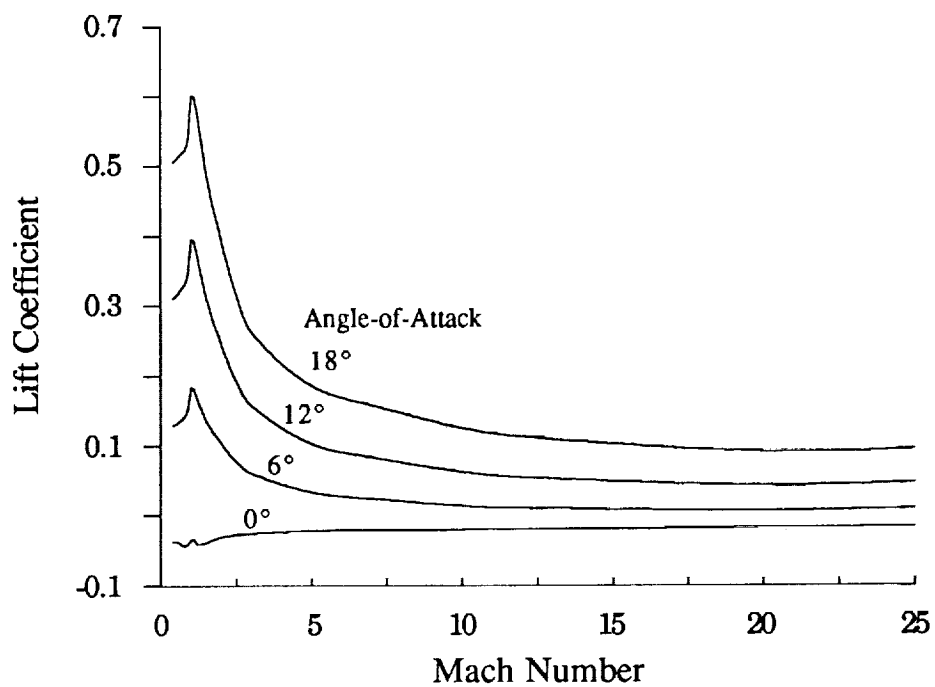
Table 5b Effect of Available Thrust Level ($a_{\max} = 3$ g's)

A_{comb} (ft ²)	M_{switch}	h_{switch} (ft)	q_{peak} (lb _f /ft ²)	m_{final} (slugs)	t_{final} (sec)
400	6.59	100,987	1,025	5,844	557.1
275	6.60	94,936	1,087	5,776	614.6
180	6.59	84,252	1,650	5,641	739.4

Table 5c Effect of Specific Impulse ($a_{\max} = 3$ g's)

I_{sp} (%)	M_{switch}	h_{switch} (ft)	q_{peak} (lb _f /ft ²)	m_{final} (slugs)	t_{final} (sec)
100	6.59	100,987	1,025	5,844	557.1
80	6.59	101,045	1,028	5,245	549.7
60	6.60	101,240	1,029	4,382	539.1

GHAME AERODYNAMICS



GHAME AERODYNAMICS

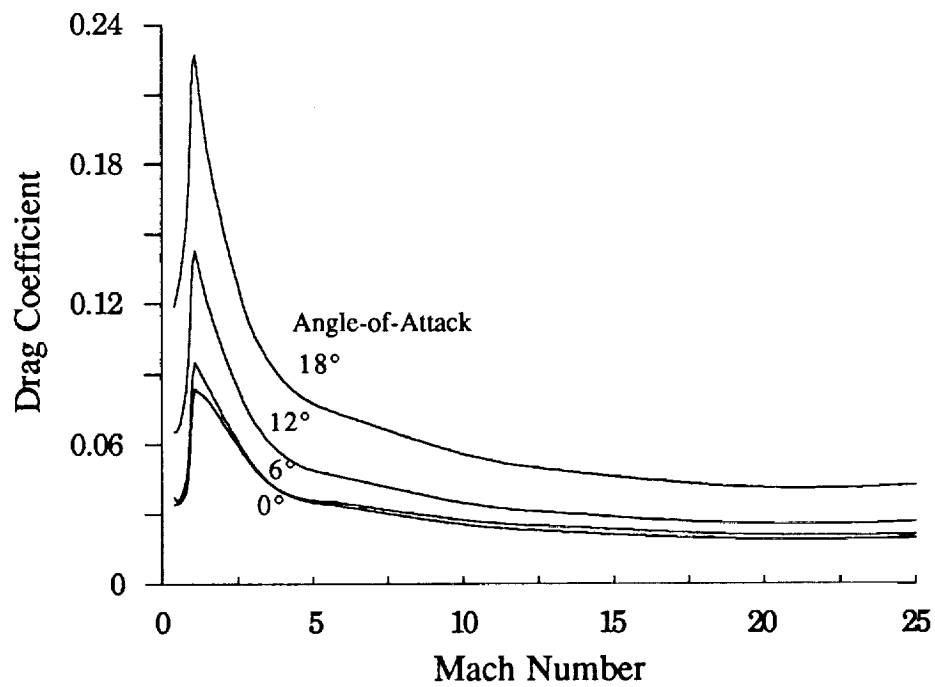


Figure 1 Aerodynamic Characteristics

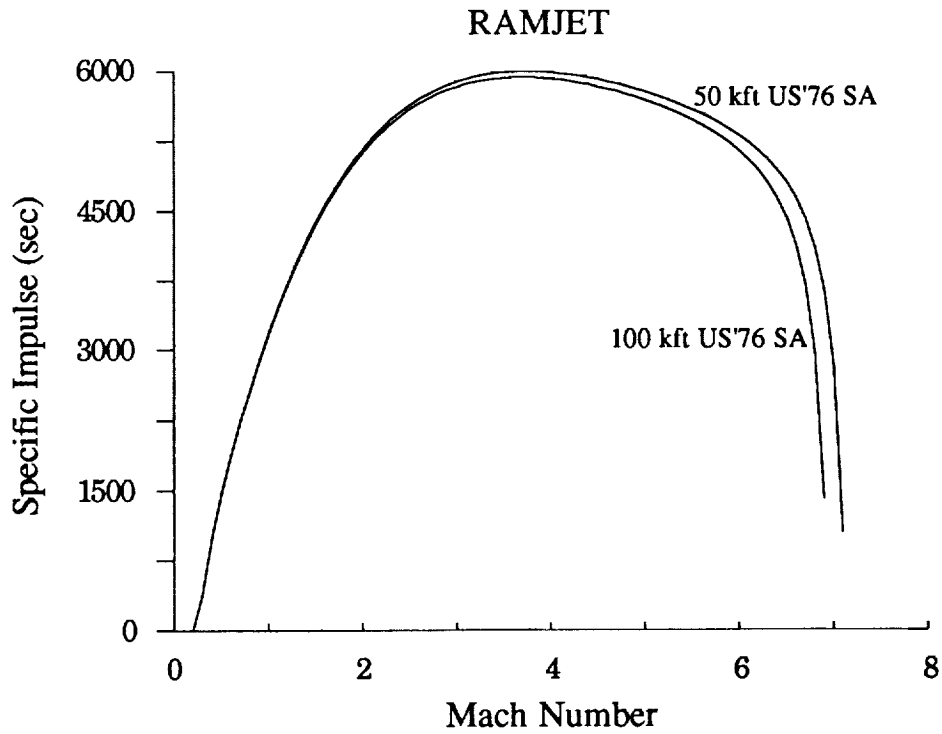
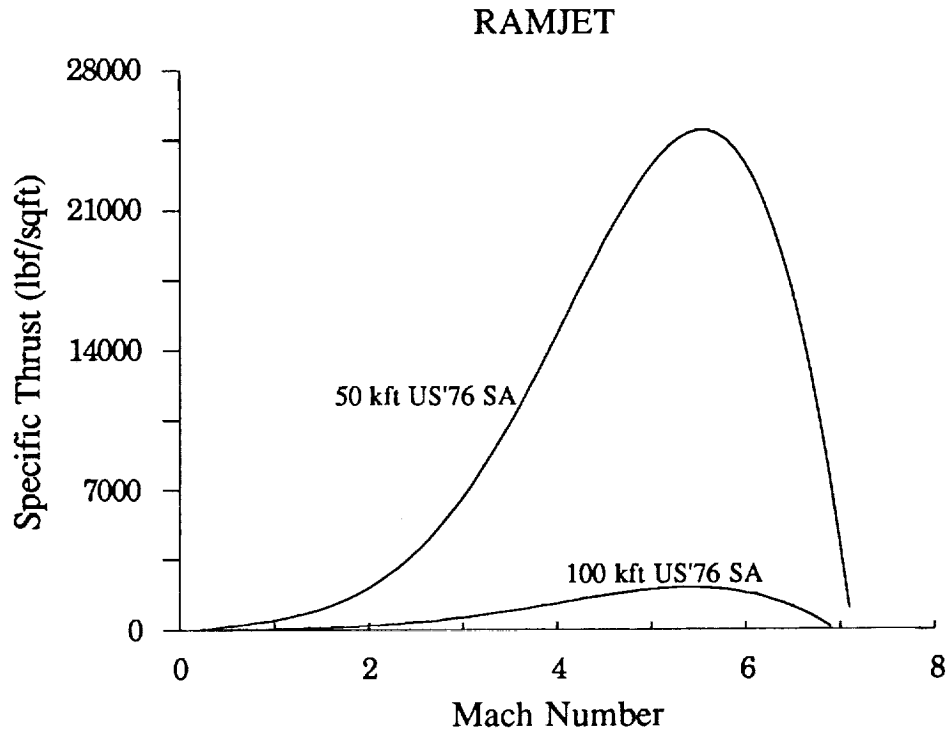


Figure 2 Ramjet Characteristics

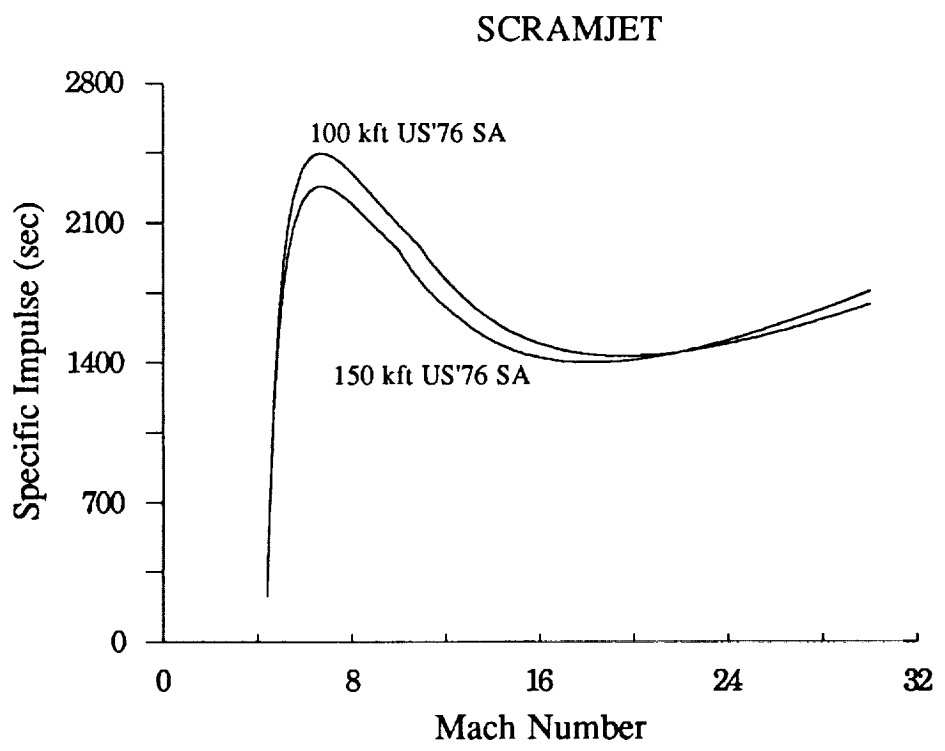
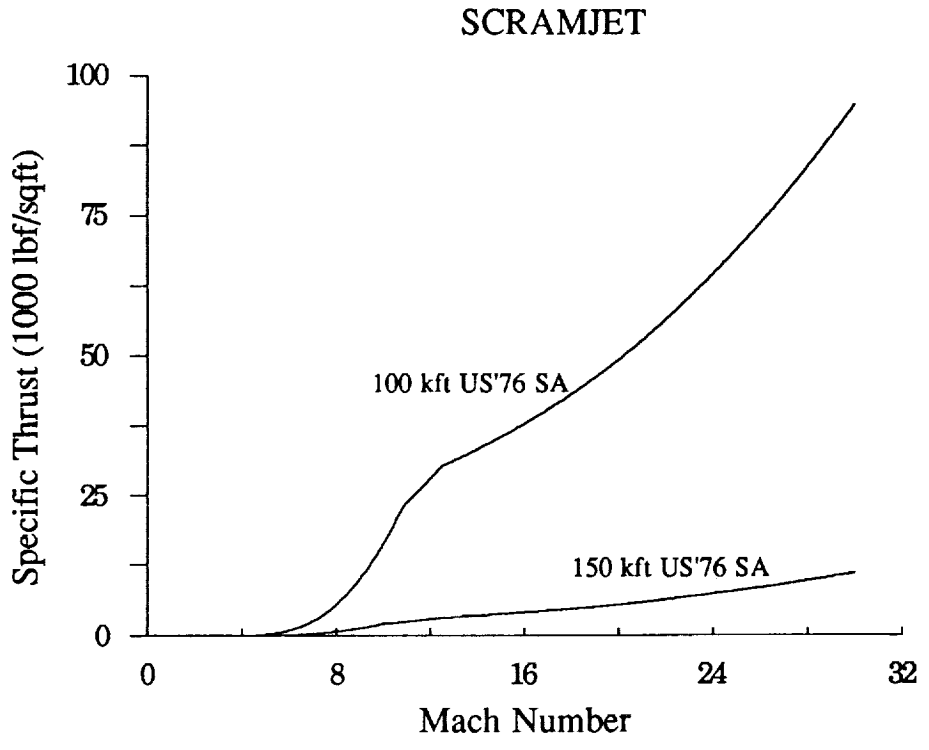


Figure 3 Scramjet Characteristics (Original Model)

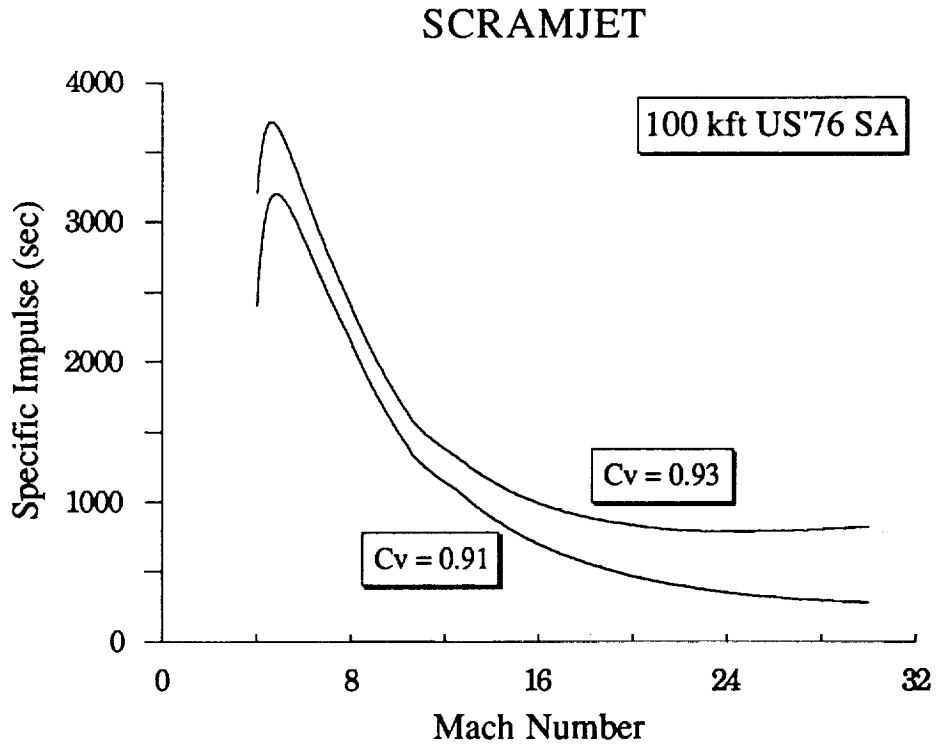
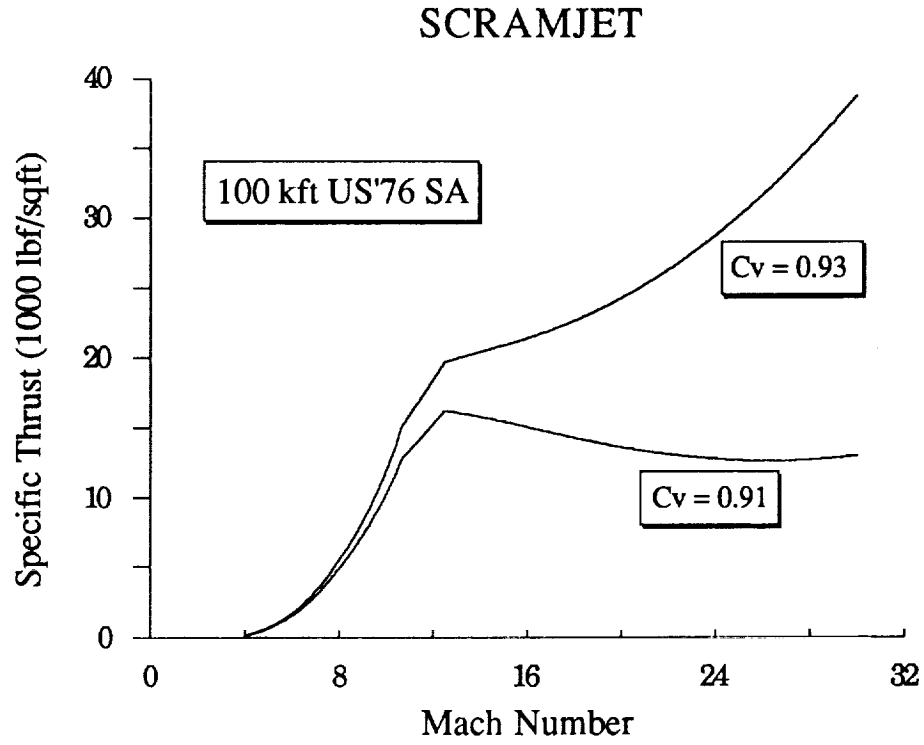


Figure 4 Scramjet Characteristics (Revised Model)

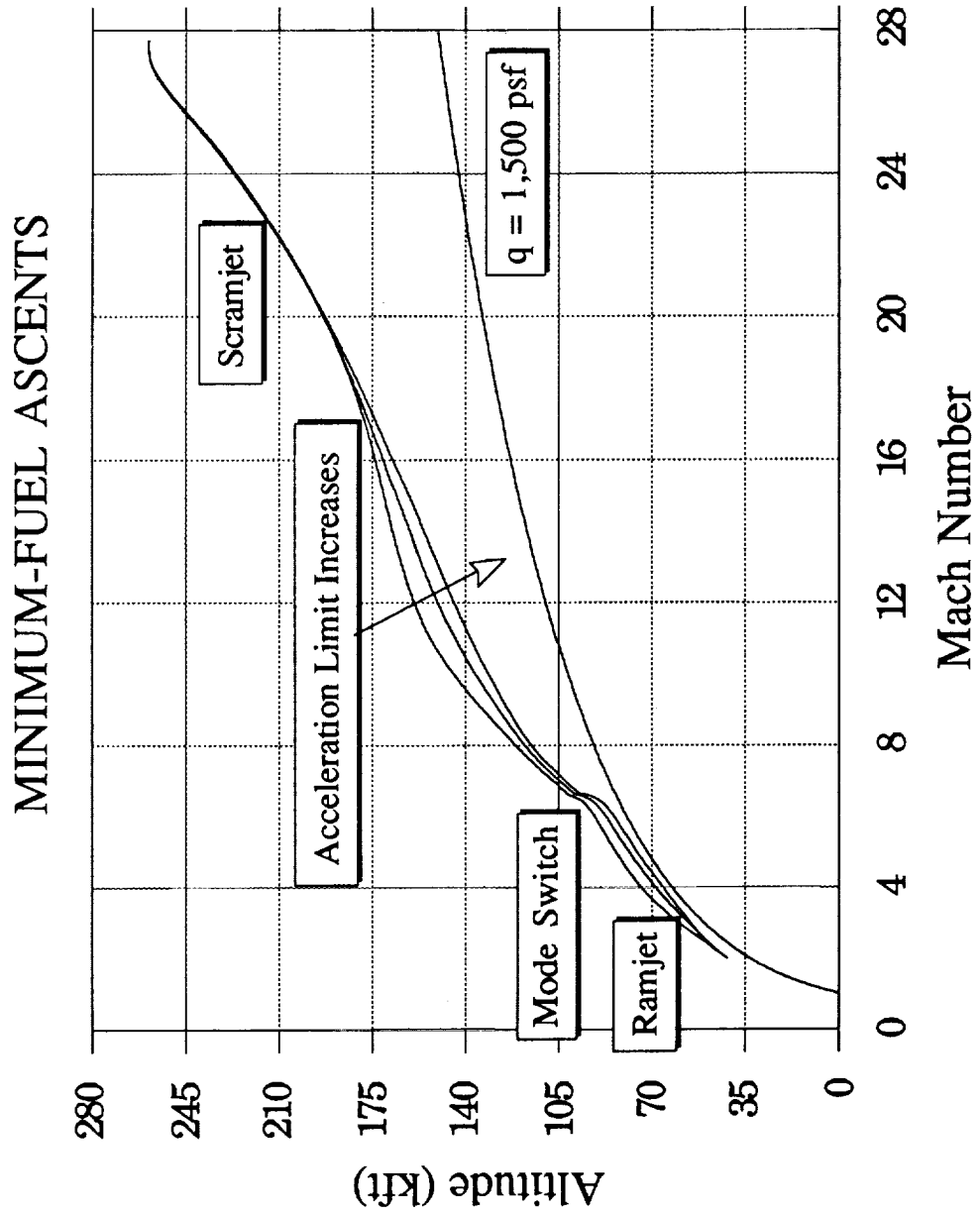


Figure 5 Effect of Acceleration Constraint on the Altitude Profile

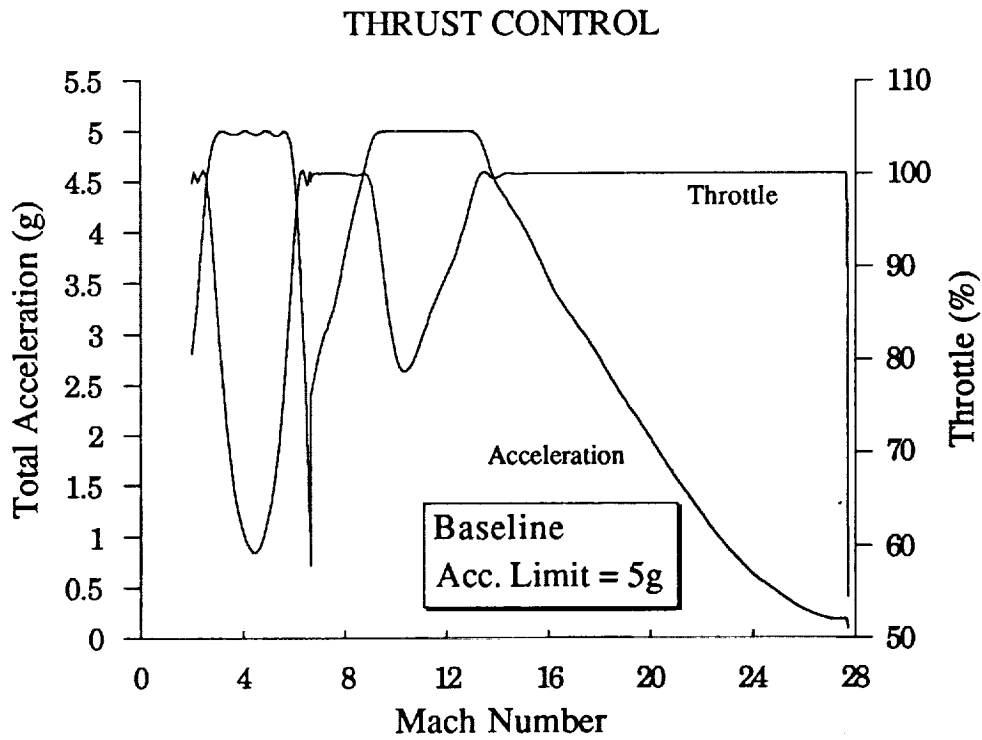
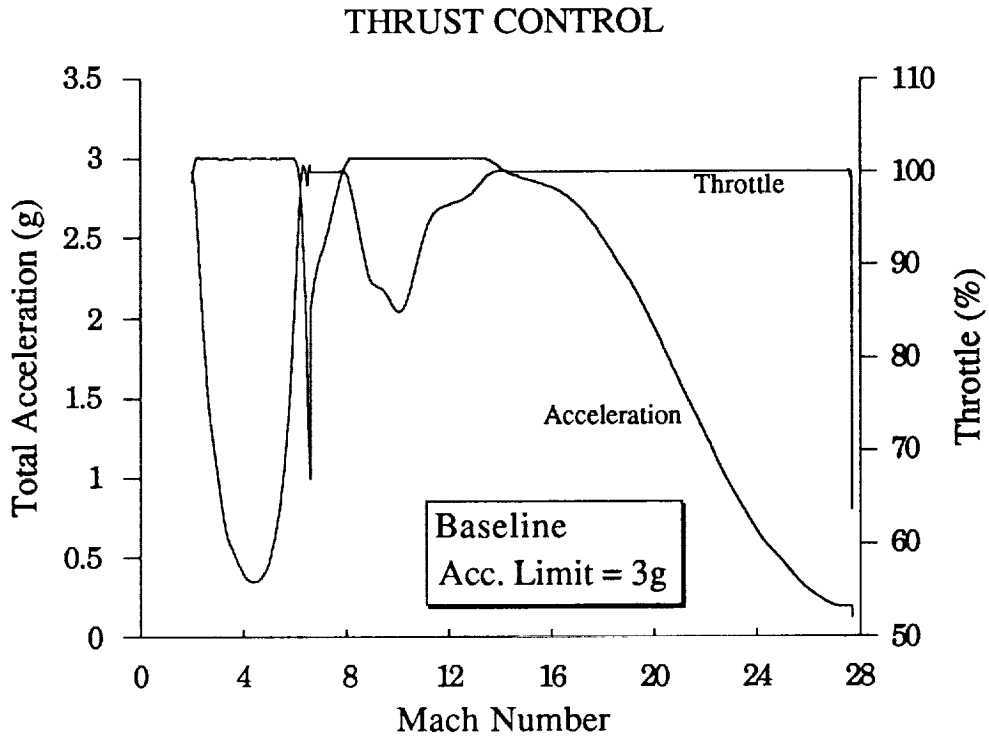


Figure 6a and b Thrust Control for Minimum-Fuel Ascent

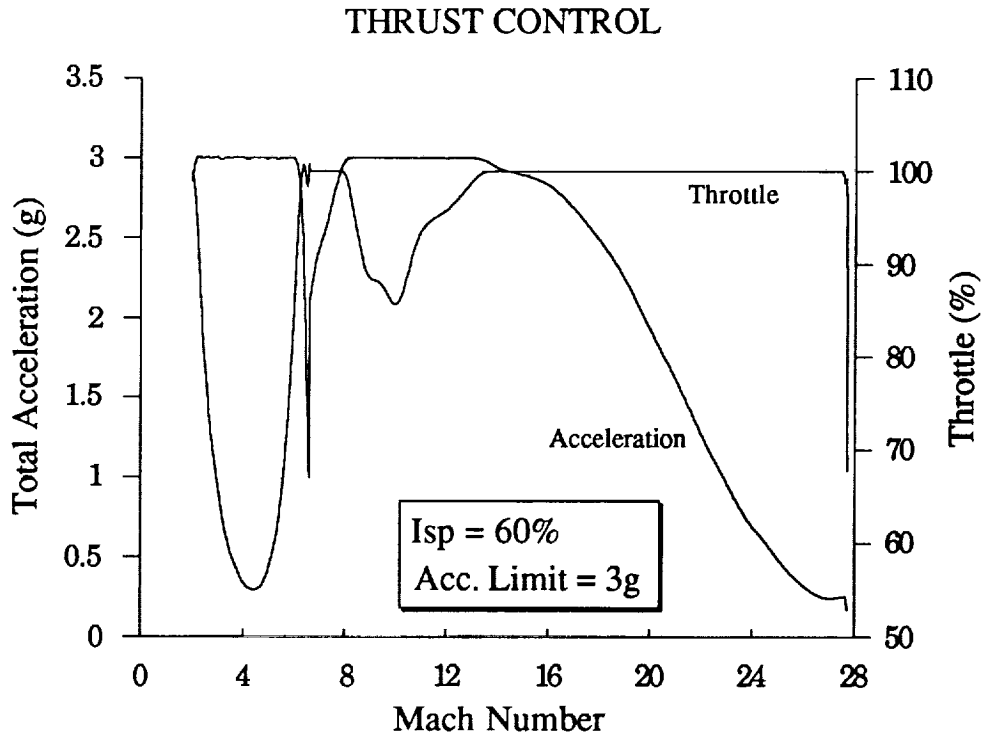
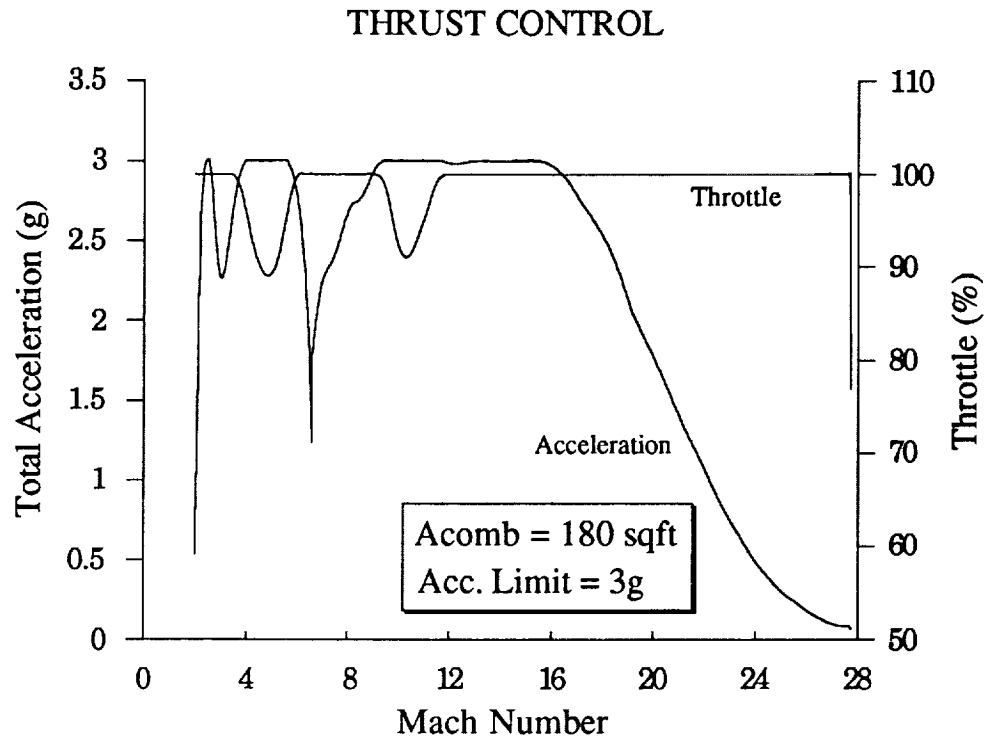


Figure 6c and d Thrust Control for Minimum-Fuel Ascent

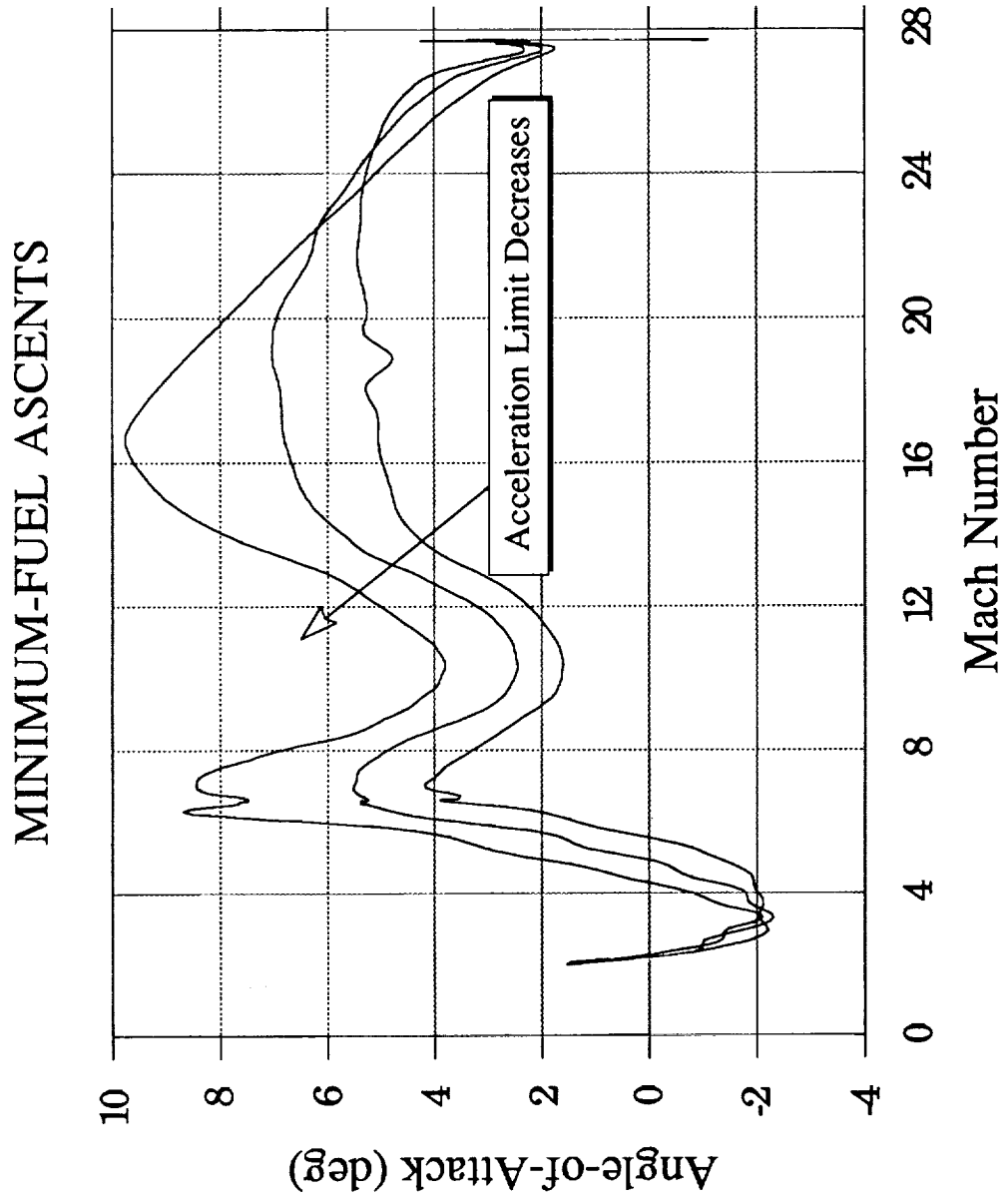


Figure 7 Effect of the Acceleration Constraint on the Angle-of-Attack

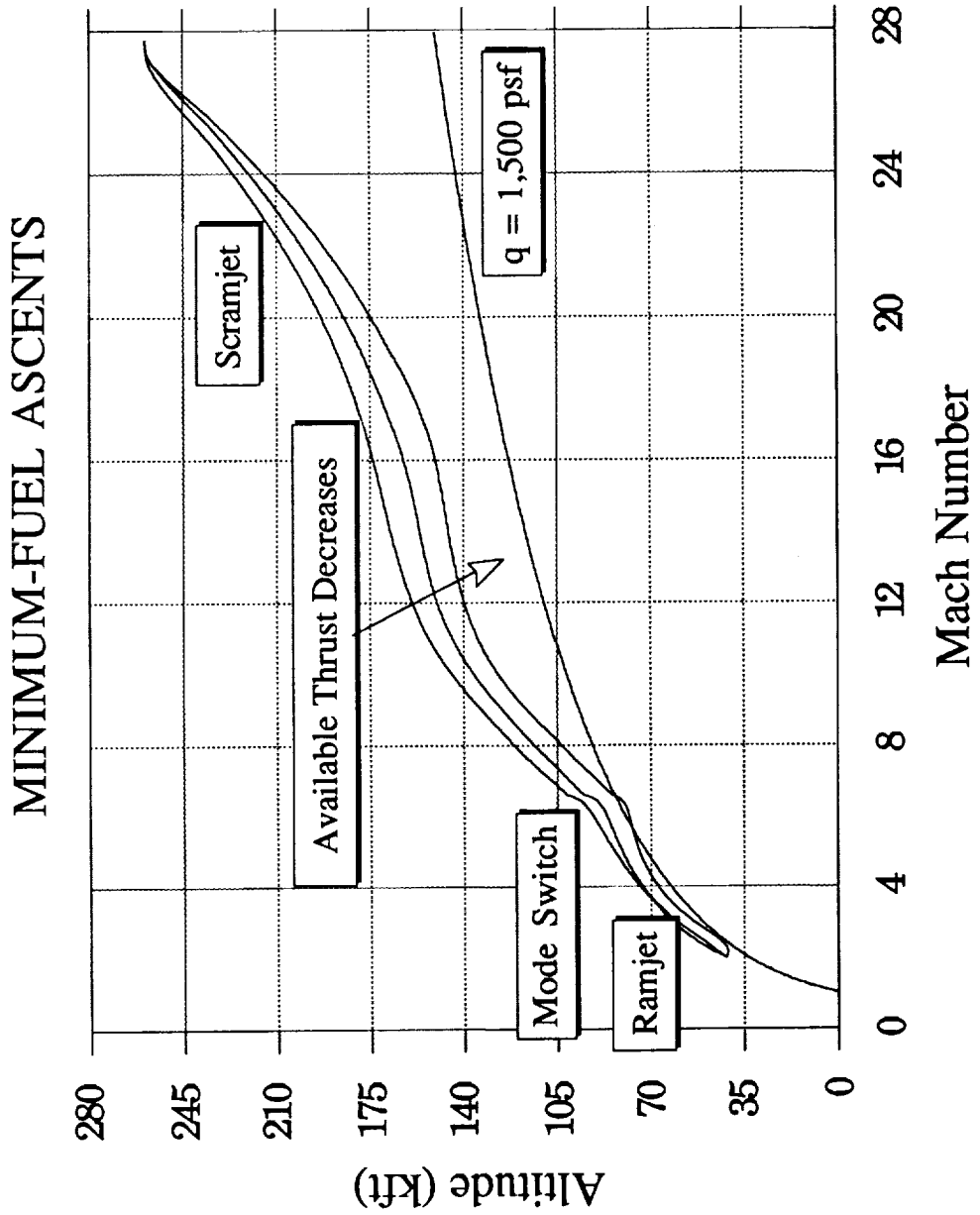


Figure 8 Effect of Available Thrust Level on the Altitude Profile

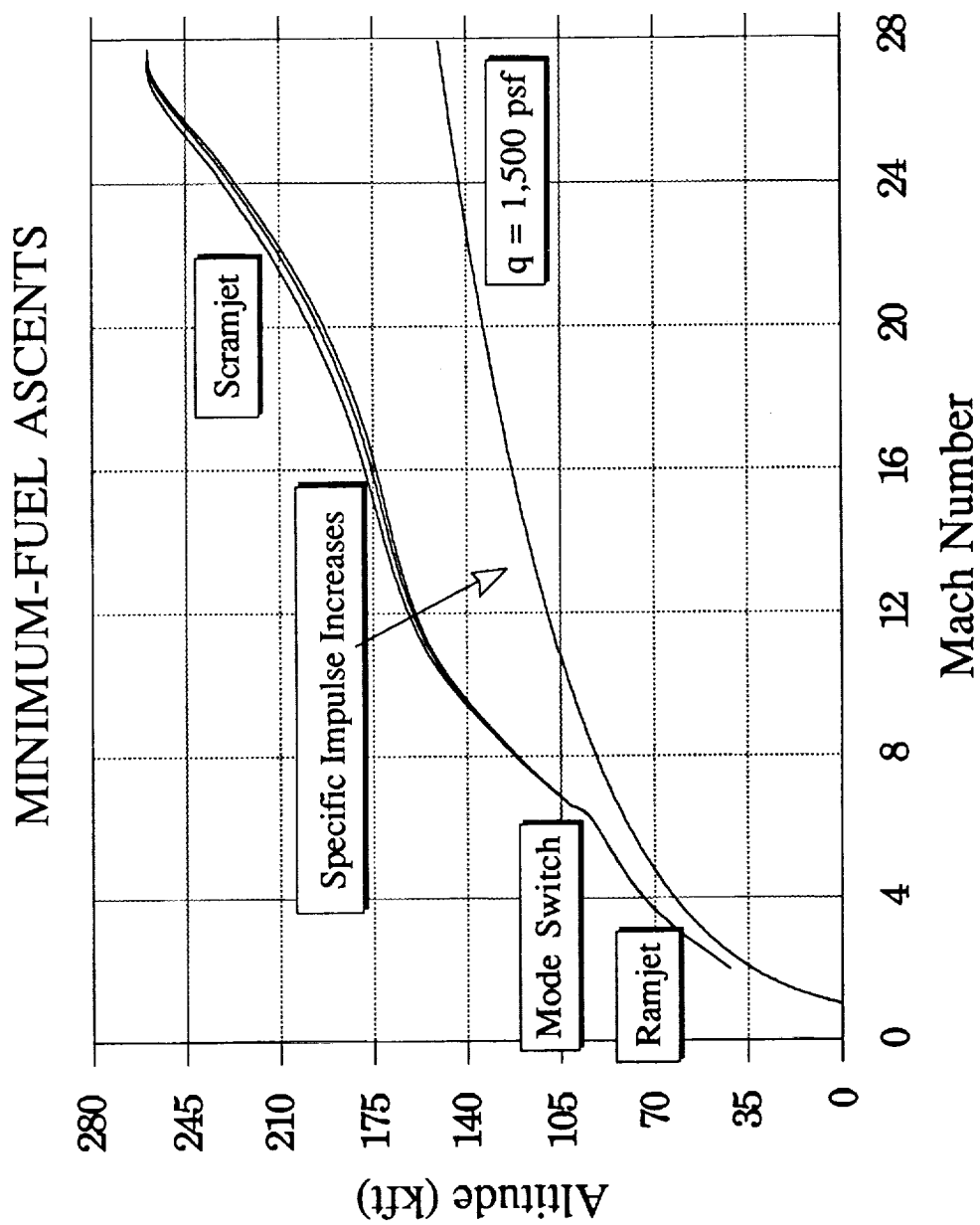


Figure 9 Effect of Fuel Specific Impulse on the Altitude Profile

APPENDIX

A.0 INTRODUCTION

The purpose of this propulsion model is to render the maximum thrust (T) and specific impulse (I_{sp}) as a function of Mach number (M) and altitude (h) in a standard atmosphere, covering the entire flight envelope of an air-breathing SSTO vehicle.

The aero-engine for such a vehicle comprises several distinct propulsion modes, each suited to operate over a specified speed range. The propulsion model consists of an afterburning single-flow turbojet, a ramjet and a scramjet. The mechanical details of how these modes are to be integrated into one device will not be discussed in what follows. It is tacitly assumed that such an engine can be construed.

The respective modes are analyzed using simple one-dimensional flow analysis for perfect gasses, employing constant efficiencies throughout the engine. The key however, is to use the most appropriate ones, i.e. to use those efficiencies that remain more or less constant over the operating range.

A.1 AMBIENT AND FREE-STREAM CONDITIONS

The ambient conditions, i.e. pressure (p_a), temperature (T_a) and speed of sound (a), are completely determined by the altitude in a standard atmosphere. In the current implementation, the U.S. Standard Atmosphere, 1976 is being used [4].

The ambient conditions together with the free-stream Mach number determine the free-stream stagnation pressure (p_{t0}) and stagnation temperature (T_{t0})

$$p_{t0} = p_0 \left(1 + \frac{\gamma - 1}{2} M^2 \right)^{\frac{\gamma}{\gamma - 1}} \quad T_{t0} = T_0 \left(1 + \frac{\gamma - 1}{2} M^2 \right) \quad (A1)$$

A.2 THE AFTERBURNING TURBOJET

The basic components of a afterburning turbojet (Figure A1) consist of an intake, compressor, combustion chamber or burner, turbine, afterburner and a nozzle.

In the performance assessment of a turbojet one needs to make a distinction between the operation of the engine at its design point and away from it. Since the SSTO vehicle is accelerating to Earth-orbit, it operates over a wide range of velocities and altitudes. The off-design operation of the engine is therefore its "true" operating condition and should be satisfactorily modeled.

First, the design point operation is analyzed for fixed design parameters such as compressor pressure ratio ($\epsilon_{c,des}$), turbine entry temperature (TET) and nozzle expansion ratio. Subsequently, using some realistic assumptions about the turbojet operation, estimates can be found for the off-design compressor pressure ratio (ϵ_c) and ditto mass flow (m), which are adequate for this simple model.

A.2.1 The Intake

The intake compresses the air and reduces its velocity, thereby raising its static temperature. In general, the Mach number should be in the range of 0.3 to 0.5 at the compressor inlet. The intake-diffusion is assumed to be adiabatic, since the diffusion takes place very rapidly. Hence the stagnation temperature remains constant, that is $T_{t2}=T_{t0}$.

Due to imperfect diffusion, a drop in stagnation pressure will generally occur. At high velocities the intake efficiency is best specified by a constant kinetic efficiency

$$\eta_{KE} = \left[\frac{(V_{is})^2}{V_0^2} \right]^2 \quad (A2)$$

For a well designed intake $\eta_{KE} \approx 0.94$ to 0.97 , [13,16]. The intake pressure recovery ratio is then specified by

$$\eta_R = \frac{P_{t2}}{P_{t0}} = \left(1 + (1 - \eta_{KE}) \frac{\gamma - 1}{2} M_0^2 \right)^{-\frac{\gamma}{\gamma - 1}} \quad (A3)$$

During off-design operation a fixed-geometry intake would incur spillage drag as a consequence of changes in the mass flow, in addition to a reduction in efficiency. However, here it is reasonable to assume that for such an advanced vehicle as an aerospace plane, a sophisticated variable-geometry intake will be installed, to avoid spillage drag while providing the mass flow to match the engine. In other words, in the current model it is assumed that the intake itself does not exhibit any off-design behavior (easier stipulated than realized).

A.2.2 The Compressor

The compressor provides an additional rise in pressure. The compressor pressure ratio is a design parameter.

$$\left[(\epsilon_c)_{des} \right]_{0mSA, static} \approx 15$$

according to [16].

Assuming a constant engine speed, there is a constant volume flow through the engine due to the constant axial velocity through the compressor [13]. Employing a constant isentropic compressor efficiency ($\eta_c=0.96$), it can be shown that the off-design pressure ratio is given by

$$\epsilon_c = \left(1 - \eta_c + \sqrt{\eta_c^2 + \frac{T_{0mSA}}{T_{t0}} D} \right)^{\frac{\gamma}{\gamma - 1}} \quad (A4)$$

where

$$D = \left(\epsilon_c^{\frac{\gamma}{\gamma-1}} - 1 \right) \left(2\eta_c + \epsilon_c^{\frac{\gamma}{\gamma-1}} - 1 \right) \quad (\text{A5})$$

A constant isentropic efficiency has been used as opposed to the more suitable (i.e. more realistically constant) polytropic efficiency, in order to be able to obtain a closed-form expression for the pressure ratio.

The compressor exit temperature (T_{t3}) is determined by

$$T_{t3} = T_{t2} \left(1 + \frac{\epsilon_c^{\frac{\gamma}{\gamma-1}} - 1}{\eta_c} \right) \quad (\text{A6})$$

The constant volume flow, combined with a constant intake delivery speed of 150 m/s to 170 m/s [18], allows one to determine the specific mass flow per unit compressor area

$$\frac{\dot{m}}{A_c} = \frac{P_2}{RT_2} V_2 \quad (\text{A7})$$

Thus, as will become apparent later, the compressor inlet area constitutes the engine sizing parameter which scales the thrust linearly.

A.2.3 The Combustion Chamber

In view of its purpose, this model is not concerned with the intricacies of the combustion process itself. Instead, simple heating relations for a perfect gas are used with a given heating value of the fuel. In this particular case, hydrogen is used in all three propulsion modes.

For maximum thrust, heat must be added up to the limit set by the TET, approximately 1600 to 1700 K. For the specific fuel flow one obtains

$$f_b = \frac{TET - T_{t3}}{\frac{\eta_b H}{c_p} - TET} \quad (\text{A8})$$

The burning efficiency η_b is a correction factor for imperfect combustion, a typical value is 0.96 [13,17]. H is the heating value of the fuel, $H \approx 144.6 \cdot 10^6$ J/kg. An inevitable by-product of the heat addition is a loss in stagnation pressure. A reasonable estimate is 3% to 7%. [13].

A.2.4 The Turbine

In the turbine the gas provides the work needed for compression.

$$c_{p_{\text{air}}} (T_{t3} - T_{t2}) = \eta_m c_{p_{\text{gas}}} (1 + f_b) (TET - T_{t5}) \quad (\text{A9})$$

where η_m represents a mechanical efficiency factor for the turbo-machinery, $\eta_m \approx 0.99$. Employing constant isentropic turbine efficiency η_t , the pressure ratio is determined by

$$\frac{p_{t5}}{p_{t4}} = \left(1 - \frac{TET - T_{t5}}{\eta_t TET} \right)^{\frac{\gamma}{\gamma-1}} \quad (A10)$$

A.2.5 The Afterburner

The afterburner increases the specific thrust considerably, an important consideration for a boost vehicle like an aerospace plane. Since the afterburner is not followed by any rotating machinery the exit temperature ($T_{t\text{exit}}$) can be higher than the TET. A reasonable value is 2000 K, [16].

The specific fuel flow is given by

$$f_{ab} = \frac{T_{t\text{exit}} - T_{t5}}{\eta_b H} (1 + f_b) \frac{c}{p_{av}} - T_{t\text{exit}} \quad (A11)$$

Again, a slight drop in stagnation pressure is inevitable.

A.2.6 The Nozzle

A straightforward sensitivity analysis will show that, for optimal performance, one needs to install a convergent-divergent nozzle (also known as a condi nozzle) on a high performance vehicle, in order to let the gas expand to near ambient pressure. The decrease in performance, using only a convergent nozzle becomes especially noticeable at supersonic speeds. However, an upperlimit should, realistically, be imposed on the expansion ratio $ER = A_{\text{exit}}/A_{\text{throat}}$ in accordance with engine size limitations.

From the known mass flow through the engine one can determine the necessary throat size

$$\frac{A_{\text{throat}}}{A_c} = \frac{m}{A_c} (1 + f_b + f_{ab}) \frac{\sqrt{T_{t\text{exit}}}}{p_{t\text{exit}}} \sqrt{\frac{R}{\gamma}} \left(\frac{\gamma+1}{2} \right)^{\frac{\gamma+1}{2(\gamma-1)}} \quad (A12)$$

Both the ideal expansion and the given mass flow imply a continuously adjustable nozzle geometry. The exit Mach number is determined from either

$$M_{\text{exit}}^2 = \frac{2}{\gamma-1} \left[\left(\frac{p_{t\text{exit}}}{p_0} \right)^{\frac{\gamma-1}{\gamma}} - 1 \right] \quad (A13)$$

for ideal expansion $p_{\text{exit}} = p_0$, or

$$ER = \frac{1}{M_{\text{exit}}} \left(\frac{1 + \frac{\gamma-1}{2} M_{\text{exit}}^2}{\frac{\gamma+1}{2}} \right)^{\frac{\gamma+1}{2(\gamma-1)}} \quad (\text{A14})$$

for maximum expansion, where the maximum expansion ratio (ER) is determined from

$$ER = \frac{A_{\text{exit}}}{A_c} \frac{A_c}{A_{\text{throat}}}$$

where A_{exit}/A_c is determined by the engine size and is taken to be approximately 4.0. Subsequently, the exit velocity is determined from

$$w_{\text{exit}} = C_v M_{\text{exit}} \sqrt{\frac{\gamma R T_{t_{\text{exit}}}}{1 + \frac{\gamma-1}{2} M_{\text{exit}}^2}} \quad (\text{A15})$$

where the nozzle velocity factor $C_v \approx 0.96$ is introduced to adjust for nozzle losses. The thrust per unit of compressor inlet area is determined from

$$\frac{T}{A_c} = \frac{\dot{m}}{A_c} [w_{\text{exit}} (1 + f_b + f_{ab}) - V_0] + ER \frac{A_{\text{throat}}}{A_c} (P_{\text{exit}} - P_0) \quad (\text{A16})$$

and the specific impulse is given by

$$I_{\text{sp}} = \frac{\frac{T}{A_c}}{g_0 \frac{\dot{m}}{A_c} (1 + f_b + f_{ab})} \quad (\text{A17})$$

A.3 THE RAMJET

The ramjet is more or less a skeleton turbojet with the turbo-machinery taken out since there is no need for a compressor, the ram compression by itself is effective enough. The ramjet consists of an intake, a combustion chamber and a nozzle. All pertinent equations for these components are stated in the previous section on the afterburning turbojet. A number of (small) changes in some parameter values have been applied, consistent with the different operating range of the engine.

The intake delivery Mach number has been set to a constant value of 0.5. The massflow equation (A7) must now be restated in terms of constant intake delivery Mach number

$$\frac{\dot{m}}{A_c} = \sqrt{\frac{\gamma}{R}} \frac{P_2}{\sqrt{T_2}} M_2 \quad (\text{A18})$$

The exit temperature has been raised to 2500 K, while the nozzle exit to combustor inlet area ratio A_{exit}/A_c has been raised to 6.0 to boost performance.

A.4 THE SCRAMJET

The scramjet is very similar to the ramjet. The main difference is that the combustion takes place while the air is moving at supersonic velocities. The reason to apply supersonic combustion is to avoid the excessive losses in stagnation pressure, which are introduced first, when the air is decelerated by means of an intake to subsonic velocities for combustion, and afterwards, when it is accelerated again by means of a nozzle to supersonic velocities. A schematic diagram of a scramjet is presented in Figure A2.

A.4.1 The Intake

For operation at very high velocities reference [14] suggests using a different type of process efficiency, which more nearly stays constant: $K_D \approx 0.93$. It can be shown that the kinetic efficiency is related to K_D by

$$\eta_{KE} = K_D + (1 - K_D) \left(\frac{V_3}{V_0} \right)^2 \quad (\text{A19})$$

and η_{KE} determines the recovery pressure ratio in the usual way. Additionally, the intake delivery Mach numbers are now supersonic. The recommended diffusion ratio M_0/M_3 is about 3.0 for optimal fuel specific impulse.

A.4.2 The Combustion Chamber

Combustion in a combustor with constant cross section area leads to adequate performance at high speeds. However, at the lower speed range constant cross section area combustion leads to thermal choking and rapid degradation of performance. To avoid this one needs to employ a variable cross section area combustor. A straightforward implementation of such a scheme however, would increase the complexity of the model beyond the sought after relative simplicity. A particularly elegant way to circumvent this problem is to employ the following relation between static pressure and combustor area

$$\frac{P_5}{P_3} = \left(\frac{A_5}{A_3} \right)^{\frac{E}{1-E}} \quad (\text{A20})$$

Setting E equal to 1.0, one obtains the constant cross section area flow, while setting E equal to 0.0 results in constant pressure flow, which in principle cannot choke. By using the above relation with linearly increasing E from 0.0 to 1.0 over the Mach number range from 3.0 to 11.0, one can alleviate the performance degradation.

The equations for one-dimensional flow with heat addition employing (A20) can be found in [13]. Given the initial state (M_3 , p_{t3} , T_{t3}) and a certain heat input as determined by the fuel-to-air ratio f_b , the final state (M_5 , p_{t5} , T_{t5}) can be found.

$$T_{t5} = \frac{T_{t3} + \frac{\eta_b H}{c_{p_{av}}} f_b}{1 + f_b} \quad (\text{A21})$$

The Mach number at the burner exit can be found from

$$\frac{T_{t5}}{T_{t3}} = \left(\frac{M_5}{M_3} \frac{E + \gamma M_3^2}{E + \gamma M_5^2} \right)^2 \frac{1 + \frac{\gamma-1}{2} M_5^2}{1 + \frac{\gamma-1}{2} M_3^2} \quad (\text{A22})$$

and the stagnation pressure from

$$\frac{p_{t5}}{p_{t3}} = \left(\frac{E + \gamma M_3^2}{E + \gamma M_5^2} \right)^E \left(\frac{1 + \frac{\gamma-1}{2} M_5^2}{1 + \frac{\gamma-1}{2} M_3^2} \right)^{\frac{\gamma}{\gamma-1}} \quad (\text{A23})$$

An optimal fuel-to-air ratio as a function of free-stream Mach number is obtained from Swithenbank [Fig. 10, Ref. 14]. Therefore the final state of the gas can be determined. In case the fuel mixture scheme leads to thermal choking the amount of fuel is reduced to the critical amount. The critical fuel-to-air ratio is determined employing (A20) and (A21) in reverse order, substituting $M_5=1.0$ into (A21) to obtain T_{t5} and using (A20) next to evaluate f_b . The supersonic combustion process, i.e. adding heat at supersonic velocities, leads unavoidably to a large stagnation pressure loss. However the loss is significantly smaller than if subsonic combustion had been used.

A.4.3 The Nozzle

In this case, since the flow is already supersonic, the nozzle consists of a divergent section only. Again, as with the turbojet and ramjet, the expansion ratio is limited. A value of 6.0 for the A_{exit}/A_c ratio seems reasonable (cf. [15]). The exit Mach number is determined from

$$\frac{A_{\text{exit}}}{A_c} = \frac{M_5}{M_{\text{exit}}} \left(\frac{1 + \frac{\gamma-1}{2} M_{\text{exit}}^2}{1 + \frac{\gamma-1}{2} M_5^2} \right)^{\frac{\gamma+1}{2(\gamma-1)}} \quad (\text{A24})$$

and the exit velocity is determined from the pertinent equation as stated in the turbojet nozzle section. The same remark applies to the specific thrust (here, referenced to the combustor cross section area) and the I_{sp} .

A.5 CONCLUSION

Again, it should be stressed that the described model is one of relative simplicity and it does not occupy itself with the particular details of engine design. However, it adequately describes the tendencies of a true multi-mode engine and provides us with a sufficient number of parameters to tinker with and refine the modeled engine behavior over a wide range of vehicle operating conditions.

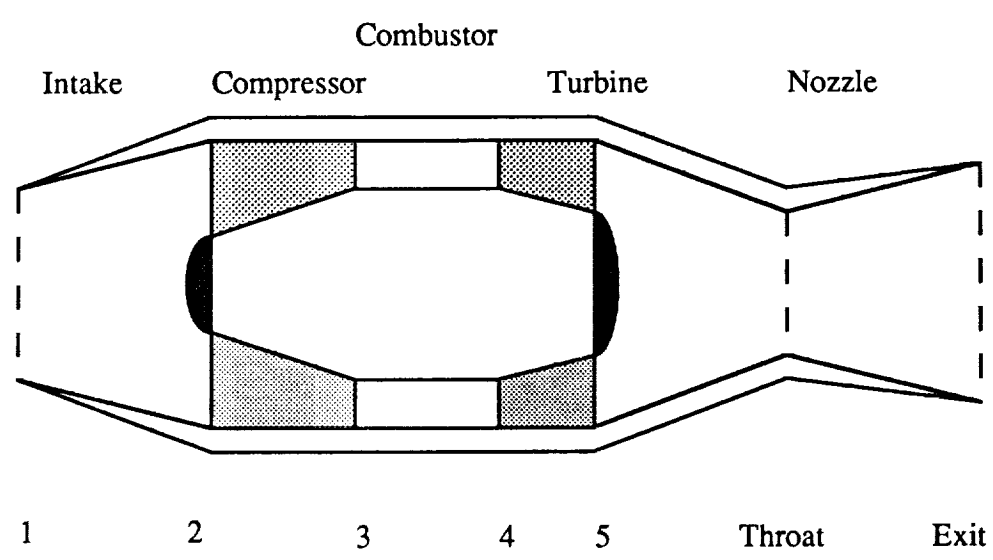


Figure A1 Basic Components of a Turbojet

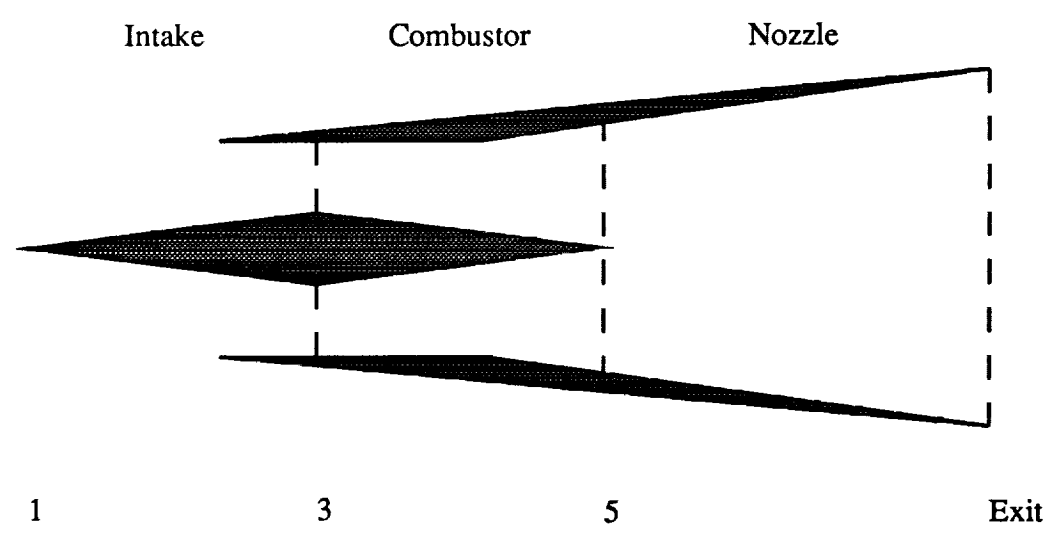


Figure A2 Basic Components of a Scramjet